Nanotechnology related to electrocatalysis for energy conversion and environmental processes

Bock, C.; MacDougall, B.; Halverson, H.

Publisher's version / Version de l'éditeur:

Handbook of Electrochemical Nanotechnology, pp. 1-29, 2006

CHAPTER 11

Nanotechnology Related to Electrocatalysis for Energy Conversion and Environmental Processes

C. Bock, B. MacDougall, H. Halverson

National Research Council of Canada, Institute for Chemical Process and Environmental Technologies, Montreal Road, Ottawa, Ontario K1A 0R6, Canada

CONTENTS

1. INTRODUCTION

Nanometer-sized metal particles are very important for heterogeneous catalysis for gas-phase reactions as well as for liquid-phase reactions. In case of the latter processes, their role in electrocatalysis for energy conversion and electrochemical pollution treatment is of special interest. Indeed, nanocatalysts are gaining more and more relevance for technical processes with significant industrial applications. Typical examples are nanosized Pt-based catalysts for H_2, CO, and CH_3OH oxidation and the O_2 reduction reaction for low-temperature fuel cells. Another area of interest is the water splitting reaction, i.e., the generation of H_2 and O_2 where high surface area electrocatalysts of three-dimensional structures are used. In more recent years, electroorganic synthesis and electrochemical processes to treat environmental pollution problems have also gained interest. Examples are the removal of organic pollutants from wastewater streams, where the organic toxins are either transferred into useful products or

ISBN: 1-58883-039-X/$35.00

Handbook of Electrochemical Nanotechnology
Edited by Yuehe Lin and Hari Singh Nalwa
Pages: 1–29

less toxic materials or collected at high surface area carbon substrates. In the majority of these cases, the electrode surface structure and chemical nature plays an important role, as they influence the product distribution and efficiency of the electrochemical process. Nanosized catalysts are well-known to exhibit unique physical and chemical properties, i.e., to differ from properties of the bulk metal or alloy. Despite this well-known fact, a thorough understanding of the behavior and properties of nanosized catalysts is still lacking. This is partly due to the fact that a number of properties change when the catalyst particle size decreases below about 10 nm. Additionally, a second metal that improves the activity of metallic catalysts is often added, and this, hence, adds another factor of complexity. Furthermore, the nature of the substrate used to support the catalyst particles becomes more pronounced when the particle size decreases. Hence, the separation of catalyst size effects and substrate influence on the catalytic activity is an important issue that needs to be clarified for the fundamental understanding of the catalyst structure–activity relationship and the design of effective electrocatalysts in the nanosize range.

Systematic and practical synthesis routes for nanosized catalysts have not yet been fully developed and the detailed structural characterization of nanosized particles is not trivial and requires sophisticated tools. Similar to the case of heterogeneous gas phase catalysis, a maximization of catalytic sites that are located on the surface versus the number of atoms located in the bulk is attempted in heterogeneous electrocatalysis. This is done in order not to waste valuable catalyst sites. However, smaller sized catalyst particles do not necessarily correlate with better catalytic activity, in spite of the fact that the ratio of the surface versus the bulk atoms increases as the particle size decreases. This is equivalent to an increase in surface energy of the atoms, as described by the well-known Kelvin equation. Changes in the surface energy can have a significant influence on the bond strength of molecules adsorbed on the surface, and this can have either beneficial or detrimental effects on the overall reaction kinetics. In the case of a reactant species, a stronger binding energy may indeed be beneficial, while in the case of the product this would generally be detrimental. In addition, more complicated reactions like methanol oxidation can proceed via mechanisms where numerous reaction intermediates are generated. If such intermediates behave as "poisoning" species, the influence of surface energy is very obvious. Another important factor that becomes more pronounced when the number of surface versus the number of bulk atoms increases, i.e., when the particle size decreases, is the change in the number of surface atoms in a specific plane with a resulting change in catalytic activity. Interestingly, the intrinsic catalytic activity, i.e., the activity normalized for the catalyst surface area, often decreases for nanosized catalyst particles. To the best of our knowledge, there is only one system for which an apparent increase in the intrinsic catalytic activity has been reported. The results were for single nanoparticles of Pd formed on Au(111) surfaces and will be discussed in this chapter.

In this chapter, electrocatalysis for energy conversion reactions, namely, low temperature fuel cells, is first reviewed. This is followed by a discussion of electrochemistry for wastewater treatment and electrosynthesis reactions. Issues such as preparation and characterization of nanosized catalysts are addressed. The influence of the preparation method on the catalyst properties and electrocatalytic activity are also reviewed. Experimental results and observations are discussed in some detail. The topic of theoretical modeling using, e.g., *ab-initio* calculations of catalyst properties will not be covered in this chapter.

2. ELECTROCATALYSIS FOR FUEL CELLS

The potential of converting gaseous and liquid fuels, i.e., chemical energy, into electrical energy using fuel cell technology as opposed to classical combustion has been known for more than a century. Lower temperature (<ca. 140°C) fuel cell systems are also referred to as polymer electrolyte membrane (PEM) fuel cells. The reactions consist of oxidizing either H_2 or CH_3OH at the anode and reducing O_2 at the cathode.

The overall reaction scheme for the H_2/O_2 fuel cell is as follows:

$$H_2 + O_2 = H_2O$$

For CH_3OH/O_2, i.e., the direct methanol fuel cell,

$$CH_3OH + \frac{1}{2}O_2 = CO_2 + 2H_2O$$

In order to achieve "rapid" reactions rates, platinum-based catalysts are used. The structure of the catalyst surface is very important, and obviously nanosized catalysts, for which the catalyst sites are located on the surface rather than in the bulk, are used in order to achieve a high degree of exposed surface area. The catalyst structure and size is of particular importance for the CH_3OH oxidation reaction or for the H_2 fuel system when the CO impurities are present in the H_2 feed stream. The CH_3OH oxidation reaction is 1 order of magnitude slower than the H_2 oxidation reaction, and, in the second case, CO poisons the catalyst. So-called bifunctional catalysts are generally used for these reactions [1–3]. Their role is described in the following (generalized) reaction scheme for the case of the CH_3OH oxidation reaction [4]:

$$\begin{aligned} Pt + CH_3OH &= Pt\text{-}(CH_3OH)_{ads} \\ Pt\text{-}(CH_3OH)_{ads} &= Pt\text{-}(CO)_{ads} + 4H^+ + 4e^- \\ M + H_2O &\rightarrow M\text{-}OH + H^+ + 1e^- \\ Pt\text{-}(CO)_{ads} + M - OH &\rightarrow Pt + M + CO_2 + H^+ + 1e^- \end{aligned}$$

In the above equations, M is an ad-metal such as Ru, Ir, Os, etc.; alternatively, metal oxides such as WO_x or MoO_x have also been proposed. The key to successful catalysis for a fuel cell reaction, i.e., to oxidize the CH_3OH completely to CO_2 at low potentials, is the adsorption of H_2O in an "active" form on the ad-metal component. It is evident from the above reaction scheme that the adsorption site where the $-OH$ species is formed needs to be close to the site where the CO_{ads} type species is formed. Therefore, the distribution of the platinum and the ad-metal surface sites on preferably the atomic level is desired to achieve maximal turnover rates of CH_3OH molecules (or the adsorbed CO poison in

the case of reformate hydrogen) oxidized per catalyst site [3, 5, 6]. Controlled engineering of nanosized and nanostructured catalyst surfaces is evidently very important. Another important feature is the structure and design of the anode and cathode layers of a fuel cell, with all of the components therein involved.

2.1. Nanosized Supported Electrocatalysts

2.1.1. Three Phase Boundary

The benefit of dispersing noble metals on high surface area substrates, thus forming catalysts in the nanometer size range, has been known for decades [7]. The high surface area support used is typically carbon blacks, such as Vulcan XC-72R, which has a surface area of ca. 250 $m^2 g^{-1}$ and particle sizes in the 30-nm range. An obvious advantage of such systems that are commonly referred to as "supported catalysts" is the increase in the number of atoms located on the surface versus the number of atoms in the bulk. This effect becomes particularly pronounced when catalyst particles of less than 10 nm are studied. For this size range, the percentage of atoms on the surface versus the bulk increases exponentially with a decrease in particle size, and, hence, the surface area per mole of catalyst also increases exponentially. This is shown in Figure 1 for the case of platinum, assuming a spherical particle shape. In addition to the high surface area, nanosized catalysts display other potentially advantageous properties when compared to the corresponding bulk material. A very significant beneficial effect of dispersing catalysts on high surface area substrates that are subsequently formed into porous, three-dimensional electrodes is the fact that a three-phase boundary (between gas, liquid, and solid) is formed [8]. This is the case for electrochemical processes involving gaseous fuels, e.g., the air or O_2 cathode and the H_2 anode in low-temperature fuel cells. Both reactions, namely, the O_2 reduction and H_2 oxidation reactions, are quite fast and thus generally take place under mass transfer control. However, the solubility of O_2 and H_2 in an aqueous electrolyte is only roughly 10^{-4} mol liter^{-1}, i.e., fairly low. Using this solubility number and the well-known Levich equation [9], one can estimate the diffusion-limited current (which is equivalent to a maximal current) that can be achieved using a planar electrode. (A planar electrode is basically a flat electrode with little or no surface roughness.) In unstirred solutions, the low diffusion limited current results in a power output of the fuel cell of only a few watts per square meter, i.e., significantly lower than the kilowatts per square meter required for practical applications, despite the fact that the reaction kinetics are fast. Looking at the Levich equation, one sees that the diffusion-limited current is proportional to the surface area, i.e., an increase in current, and hence power output of the fuel cell, is expected for supported and highly dispersed catalysts of an electrode structure design that allows access of the fuel to the catalyst sites. Therefore, one expects that the use of porous electrodes formed using supported high surface area catalysts increases the power output of a fuel cell in proportion to increase in catalyst area. However, this is not observed, and, in fact, a greater than proportional increase in power output with catalyst surface area is actually observed. This behavior, which is induced by the presence of the three-phase boundary, has been described by Will [8]. It is related to the fact that a large current-time resistance (IR) drop builds up in the gas phase, thus limiting the electron transfer reaction taking place at the liquid and solid (catalyst) interface. In pores, a meniscus is being formed, and, hence, areas of different thicknesses of the electrolyte liquid are being generated, as demonstrated in Figure 2. In all cases, the reactant gas needs to diffuse through the liquid in order to reach the catalyst surface for the charge-transfer reaction to take place. Due to the meniscus, the distance for the gas to diffuse varies and, in fact, is very small at the edge of the solid/liquid/gas boundary. This results in a very high apparent diffusion coefficient of the gas to the catalyst

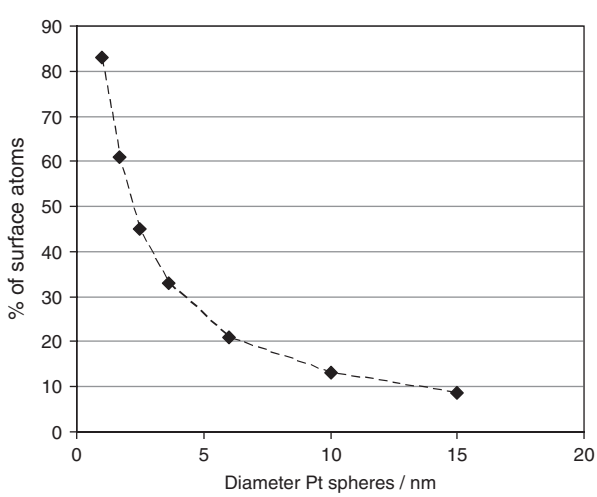

Figure 1. The calculated dependence of the percentage of atoms on the surface versus the total number of atoms for spherical platinum particles.

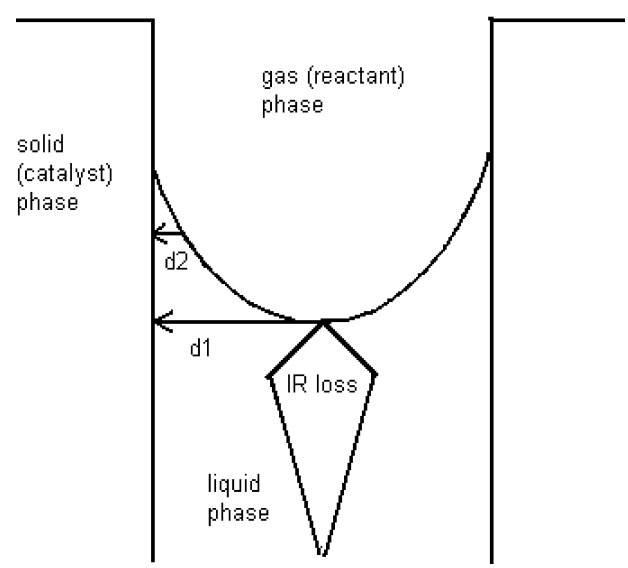

Figure 2. Schematic of a three phase (gas-solid-liquid) interface in a pore showing differences in the diffusion length (indicated in d1 and d2) of the gaseous reactant to the solid (catalyst) surface. The direction of the increase in IR (current times potential) loss along the pore is also indicated.

surface, thus high currents (order of magnitudes higher than for a planar electrode (liquid/solid interface)) are achieved. It results in effectively higher concentrations, and hence higher diffusion limited currents, than for a classical solid electrode–liquid electrolyte system.

In a fuel cell, protons are generated in the anode compartment from oxidizing either CH_3OH or H_2. The protons produced within the anode layer are transported across the membrane (typically Nafion) to the cathode compartment. For successful utilization of the cathode catalyst sites, i.e., the platinum nanoparticles, the O_2 gas as well as the protons need to access the catalyst sites, where H_2O is produced through the reaction of O_2 and the protons. The production of H_2O can lead to the well-known problem referred to as cathode flooding, i.e., the water blocks access of the gaseous fuel to the catalyst sites. Also, the water needs to be transported back to the anode electrode where it is needed for the oxidation reaction (except in the case of "pure" hydrogen). Therefore, the design of the catalyst layer of PEM type fuel cells influences the utilization of the catalyst sites as well as the power generation. The size of the carbon support particles and the resulting pore volume influences the water transport within the catalyst layers. The three-dimensional pore structure of the membrane also plays a very important role in the water management of a fuel cell. Water management of a fuel cell is important to avoid flooding as well as drying out of the membrane and electrode [10]. The influence of the pore pressure on the water evaporation rate and permeability of water has been discussed by Peled et al. [11]. They have shown that by using an inorganic membrane (a so called nanoporous proton conducting membrane) of suitable permeability, a neutral water flow can be achieved within a direct methanol fuel cell. The drawback of their system, however, is the need to introduce protons externally, i.e., H_2SO_4 solutions of high concentrations (>2 M) are needed. The influence of the pore structure of the O_2 cathode on the performance of a fuel cell has also been addressed by Holdcroft's research group [12, 13]. Their analysis incorporates a large body of theoretical work in combination with experimental data. However, only a minor (few percent) improvement in fuel cell performance was achieved by using their best-graded cathode layer as compared to the standard approach of cathode electrode layer preparation. Interestingly, the three-phase boundary appears not to be considered in the modeling work of the cathode structure. They use a macrohomogenous model considering the influence of the Nafion binder and pore volume on the O_2 and proton transport. The amount of binder (Nafion is typically used as binder and proton conductor within the catalyst layers) is varied to achieve changes in the pore volume. It has been observed that the volume of secondary pores (size range 40–200 nm) formed between agglomerates of the carbon supported catalysts is varied by changes in the catalyst layer composition, while the volume of the primary pores (20–40 nm) stays the same [14, 15]. The Holdcroft research group prepared graded cathode catalyst layers by adjusting the Nafion content. They report the best performance for a H_2/O_2 fuel cell for a layer structure of 20/30/40% Nafion. The 40% layer is the layer with the smallest agglomerate size and is located next to the membrane. The reversed arrangement consisting of a 40/30/20% Nafion layered cathode electrode structure shows poor performance. They explain the poor performance of the latter to be due to a lower O_2 and proton transport at the carbon paper/catalyst layer and the catalyst layer/membrane interface, respectively, a so-called bottle-neck effect. However, close inspection of the experimental cell potential versus current density curves could suggest large IR drop effects within this particular system. It also needs to be mentioned again that the improvement of the best 20/30/40% Nafion configuration over the nongraded 40/40/40% Nafion is only a few percent. This suggests that the grading issue itself may not be such a major factor in determining the overall system performance. Nevertheless, the work carried out by the Holdcroft group points out the important role of the pore nanostructure and pore volume on the fuel cell performance.

2.1.2. Three Phase versus Two Phase Boundary: 3M Cathode Catalyst Layer

An interesting approach involving nanostructured three-dimensional electrodes for the air (O_2) cathode for low-temperature fuel cells has been taken by Debe et al. [16] from 3M. The idea is based on achieving a higher (ideally 100%) utilization of the platinum catalyst surface sites. In a conventional fuel cell cathode only a small amount (less than 20%) of the platinum catalyst sites are utilized. This is mainly related to the large thickness of the cathode electrode layers made using the conventional approach. The thick cathode layer results in poor water management and limited accessibility (diffusion) of the gaseous O_2 fuel to the catalyst sites. At 3M, a thin film substrate (<1 μm) consisting of nanostructured whiskers has been developed. The submicrometer nanostructured substrate is much thinner (at least 10 times) than cathode electrode layers prepared using the conventional approach. The nanostructured whiskers consist of an organic pigment *N*,*N*-di(3,5-xylyl)perylene-3,4:9,10 bis(dicarboximide) (referred to as perylene red) of controllable aspect ratio (length to width) in the range of 20–50, cross-sectional dimension of roughly 50 nm, and high areal number density of $(3–5) \times 10^9$ cm^{-2}. The substrate is stable in acidic solutions. It is, however, not electronically conductive. Therefore, it is essential to coat the whiskers with a continuous layer of metal. This can be done with physical methods such as, e.g., evaporation, sublimation, sputtering, or chemical vapor deposition. High surface area catalyst substrates were prepared in this manner. According to literature data, the coated nanostructured whiskers yield electroactive platinum areas in the range 10–15 cm^2 for a Pt loading of 0.2 mg/cm^2 (geometrical area). The thickness of the platinum layer appears not to have been estimated. However, using the published data for the electroactive platinum surface per catalyst loading, a platinum layer thickness of roughly 12 nm is estimated. This is a rather thick layer of platinum considering that typically nanoparticles in the size range 2–5 nm are used in the conventional approach. Data collected under real fuel cell conditions appear to suggest that the platinum surface sites are completely utilized for the thin, submicrometer nanostructured substrate, i.e., a higher fuel cell performance per centimeter squared active platinum area is achieved with the 3M design. In fact,

the submicrometer nanostructured configuration appears to have at least a 5 times higher specific activity than the conventional platinum on high surface area carbon-based electrodes. The water generation per cathode volume is higher in the submicrometer layer 3M design. Fuel cell performance per weight of platinum data are also reported to be improved. However, the comparisons reported so far are for different conditions, namely, using different membranes. Comparisons of fuel cell performance per weight of catalyst using the different approaches to make cathodes for otherwise the same conditions are needed to further understand and to evaluate the 3M approach. Lowering the thickness of the platinum layer deposited onto the whiskers may also be desirable. However, thinner platinum layers may not be feasible, as the electrical conductivity decreases with a decrease in film thickness.

Other approaches for improving the catalyst site utilization (applied to both the anode and cathode) is to incorporate the platinum based nanosized catalyst particles into a protonically and electronically conductive polymer matrix such as polythiophene or polyaniline [17–21]. The idea is to form a continuous proton and electron conduction pathway within the electrode structure of the MEA of a fuel cell. The advantage for power generation with such a design, however, appears to be small. Furthermore, the stability of the conductive polymers is likely an issue for practical applications.

2.1.3. Particle Size Effect on Intrinsic Rate of Reaction

The dependence of the reaction rate for electrocatalytic reactions on the catalyst particle size has attracted much attention. These are studies that address fundamental questions regarding true catalytic activities. Factors discussed above, such as meniscus effects, transport limitations of fuel to the catalyst sites, and IR drop within pores, are not considered when true catalytic activities are measured. Particle size effects are particularly important for reactions that are structure sensitive, meaning that they demand catalyst sites with specific geometries. A large number of studies have been carried out for single metal platinum nanosized catalysts. Studies for bimetallic catalysts (such as Pt/Ru) also exist. However, in the latter case the studies are fewer and also subject to the fact that systematic investigations of bimetallic systems are more complicated than single metal nanosized catalysts. In addition to other properties, the catalyst particle composition may also be different as particle size varies and may be a function of the synthesis procedures. In fact, different synthetic routes are frequently used to prepare single-metal and bimetallic catalysts of different particles sizes. The need for synthetic methods that allow the tailored synthesis of nanosized catalysts of controlled size and composition is evident. The synthesis of supported metal nanoparticles with narrow size distribution is also essential in obtaining clear conclusions about structure-sensitive reactions. As discussed above, the percentage of atoms on the surface increases rapidly with a decrease in particle size below 10 nm. Hence, the strongest dependence of catalytic activity on particle size is expected for particles of less than 10 nm. In the case of platinum catalysts, a maximum in the intrinsic activity (that is, the activity per real catalyst surface area) and the mass activity (activity per catalyst weight) for both the CH_3OH to CO_2 electrooxidation reaction as well as the O_2 electroreduction reaction appears to be consistently found for particles in the 3.5–4 nm size range [22–28]. (It should be noted that the maximum intrinsic activity of nanosized platinum catalysts is always lower than the intrinsic activity for bulk metal platinum, a fact that has so far received little attention.) A decrease in the platinum particle size below the 3.5–4 nm range is reported to result in a rapid decrease of the intrinsic catalytic activity. The decrease is so pronounced that even the catalytic activity per weight of catalyst decreases with particle size. The origin of the decrease and maximum in catalytic activity is still subject to discussion and various explanations have been offered. Watanabe and Stonehart [26] proposed that the interparticle distance rather than particle size influences the measured activity for the diffusion-controlled reduction of O_2 (orr). They suggested a so-called "territory" effect to be responsible for the experimentally observed particle size effects (further discussed in Section 2.1.4).

Kinoshita offered another explanation, which is related to the thermodynamic equilibrium shape of platinum nanoparticles. The equilibrium shape of Pt nanosized particles is cubo-octahedral [27], i.e., offering a range of Pt(111) and Pt(100) surface sites. A decrease in particle size results in a lower number of surface atoms per catalyst weights in the (111) and (100) platinum crystal planes. In fact, the mass-averaged distribution (MAD) of the (100) platinum plane for a cubo-octahedral shape shows a maximum at ca. 3.5 nm, i.e., close to the experimentally reported maximum for the O_2 reduction reaction (orr). Therefore, if one considers this dependence and assumes that the (100) crystal plane for platinum is most active for the orr, the observed dependence of the orr can be explained in such a manner. However, it should be noted that this explanation is based on the thermodynamic equilibrium shape of platinum nanoparticles and it may very well be that the shape and distribution of surface atoms for platinum nanoparticles under fuel cell operating conditions are not equivalent to this shape. Furthermore, the thermodynamic equilibrium shape of platinum nanoparticles is based on particles that are not stabilized using the typical organic stabilizer molecules. The latter is a procedure frequently used for the preparation of nanosized electrocatalysts. The presence of a stabilizer, also referred to as organic ligand, can change the catalytic properties of the nanoparticle. Furthermore, it has been shown, for platinum nanosized catalysts that the shape and size of the resulting nanoparticles is influenced by the stabilizer and synthetic procedure [29], as further discussed in this chapter.

Changes in surface energy with particle size have received very little attention for the dependence of fuel cell type reactions. According to the Kelvin equation, the surface free energy (expressed in form of the vapor pressure) increases exponentially with decreasing particle size. This is shown for the case of a spherical surface in the following equation [21]:

$$\mathrm{R}T \ln \frac{P}{P^o} = \frac{2\gamma V}{r} \tag{1}$$

where R is the gas constant, T the temperature, P the pressure observed over the curved surface, P^o the normal vapor

pressure, γ the surface tension, V the volume of the spherical particle, and r the radius of the particle. The drastic changes in P (which reflects a measurement of the energetics of the surface) predicted by the Kelvin equation can have a negative or a positive effect on the catalytic activity. An increase in surface energy may result in an increase in the adsorption strength of the reactant with the catalyst surface. This would be beneficial for the adsorption of the fuel on the catalyst surface, while desorption of the product is likely more difficult. Therefore, a "Vulcano"-type dependence on particle size (instead of element) may result, i.e., where a maximum in activity is reached when the interplay between adsorption and desorption energies is optimal. An increase in surface energy also increases the susceptibility of a catalyst particle to poisoning introduced by, e.g., organics possibly present in the fuel. Hence, a decrease in the catalyst activity is expected. It should also be noted that the above form of the Kelvin equation applies to a single, i.e., isolated and unsupported, spherical particle, to be precise, a gas bubble. Deviations from this behavior may be observed for supported nanosized catalysts and supported catalysts of high loadings.

(a) O_2 Reduction Catalysts and Proposed Factors Influencing the Electrocatalytic Activity. A number of studies have been devoted to understand and explain the particle size effects of platinum catalysts that are used for the O_2 reduction reaction (orr). There are other factors, also in the nanoscale range, than the catalyst particle size that are believed to influence the catalytic activities of platinum-based catalysts for the orr. These factors are electronic (also called ligand) effects of an ad-metal acting from the bulk material through a proposed skin layer (a few monolayers thick at the maximum) of platinum on the catalyst surface. A number of studies claim a beneficial influence of platinum alloys on the orr activity [31, 32]. It has been, for example, reported that Pt alloyed with Ni, Co, and Fe shows enhanced activities for the orr. However, one needs to consider the fact that Ni, Co, and Fe are not stable in acidic solutions, particularly at high potentials, and therefore dissolve from the surface. Watanabe's research group [31, 32] reported that Pt alloys with Ni, Co, and Fe formed by sputtering show maximal orr activities at ca. 30, 40, and 50 atom% content of Ni, Co, and Fe, respectively. They reported kinetic currents that are 10, 15, and 20 times larger, respectively than for pure Pt. It is proposed that Ni, Co, and Fe leach from the catalyst surface, leaving a surface that consists of a few monolayers of Pt, i.e., a skin layer of platinum. It is further proposed that the reported enhanced catalytic activity for the orr is based on an increased d-electron vacancy of the thin Pt surface layer caused by the underlying alloy. A higher CO tolerance for the "skin-layer" catalysts is also proposed. It should be noted that the formation of a continuous skin layer of platinum on top of the alloyed phase of the catalyst is a proposition and has not actually been proven to the best of our knowledge. Furthermore, a closer inspection of their data shows that the catalytic activities of Pt for the orr reported by this group is less than reported in other studies [34–36], thus throwing into question the claimed large enhancement of the Fe-group metal alloys. In fact, great care must be taken to measure orr activities. Platinum surface sites can easily be blocked by anion adsorption (the influence of chloride is particularly strong) or Pt oxides present at the surface, resulting in a decrease in activity. Enhancements of the specific mass activity (A per mg of Pt) of the order of 3–4 times have been reported for Pt–Co and Pt–Cr nanosized catalysts supported on carbon black [35]. However, a clear problem for these Fe-group based alloy catalysts is their stability. Furthermore, it has not actually been shown that these particular alloys have better catalytic activities. Better orr activities for these catalysts have only been observed at low current densities according to Gasteiger et al. [35]. Another cause of concern is their behavior when used as real electrodes for the orr in a fuel cell. It is believed that platinum alloys with the Fe-group metals cause larger problems with regard to flooding of the cathode. This has been assigned to the increased hydrophilicity of the Fe-group metal. Water flooding of the cathode is a major problem in fuel cell operations typically resulting in very poor utilization of the catalyst sites, as discussed earlier in this chapter. Furthermore, for the successful development of new cathode catalysts, it is important to compare activities for the orr to proper experimental data for platinum. As discussed by Gasteiger et al. [35], the extraction of intrinsic current density values involves the extrapolation of 4 orders of magnitudes and can hence result in large errors. They suggested a comparison of the specific mass and specific catalyst activity at a specific potential instead. However, when using this method, one needs to keep in mind that depending on the surface area, electrode structure, and potential, other factors than the intrinsic rate constant may be playing a role. This is further discussed in Section 2.1.4.

(b) Influence of the Catalyst Particle Size on the Activity of CH_3OH and CO_{ads} Electrooxidation Reactions. There seems to be considerable agreement in the literature that the CH_3OH electrooxidation reaction for Pt only catalysts is dependent on the catalyst particle size. Reports in general appear to agree that a maximal CH_3OH electrooxidation activity (true electrocatalytic as well mass activity) is reached with a platinum particle size of ca. 3.5–4 nm. Fewer conclusive studies exist for the case of bimetallic catalysts. The lack of this information may be partly due to the lack of development of systematic bimetallic catalysts preparation procedures in the nanoscale range and the difficulty of their structural characterization. In case of the Pt/Ru carbon supported catalysts synthesized using the modified size selected synthesis method, a particle size dependence for the CH_3OH electrooxidation reaction is found, which, however, is seen to occur for particles smaller than 3.5–4 nm. The maximum appears to be around 2.5 nm. Unlike the case of the O_2 reduction reaction (for which Pt only catalysts are used in real fuel cell applications), fewer models have been developed to explain the particle size influence on the CH_3OH electrooxidation reaction. Mukerjee and McBreen carried out *in-situ* X-ray adsorption spectroscopy (XAS) measurements as a function of the Pt particles size [28]. A broad range of Pt catalyst sizes was investigated. According to TEM images before the measurements, they varied between 2.5 and 9 nm and a broad potential range was studied. Studies were carried out in 0.1 M $HClO_4$ + up to 0.3 M CH_3OH solutions. They found that as the Pt particle size was reduced below 5 nm, the adsorption strength

of H, OH, and C_1 moieties such as CO increased. Based on these results, they proposed that the reduced activity for the CH_3OH oxidation reaction with decreasing Pt particle size is due to a combination of increased adsorption strength of both CO and OH. Of course, differences in the adsorption strength of OH on platinum nanoparticles could influence the rate of the orr as well. It is noteworthy that the CH_3OH oxidation reaction is much more sluggish than the H_2 oxidation and O_2 reduction reaction and, in fact, typically takes place under activation control as compared to mass transport controlled conditions. This makes studies and comparisons of CH_3OH oxidation activities for different catalysts somewhat easier than for the H_2 oxidation and O_2 reduction reactions.

The electrooxidation behavior of adsorbed monolayers of CO (CO_{ads}) on Pt and Pt/Ru systems (bulk metals as well as nanoparticles) is frequently suggested as a surface probe for these platinum-based catalysts. The electrooxidation reaction of adsorbed CO on platinum nanoparticles has in particular been investigated by Savinova et al. [36]. Platinum nanoparticles on oxidized glassy carbon surfaces were prepared by chemically impregnating the roughened surface with a platinum precursor salt, followed by thermal decomposition and subsequent particle growth via electrochemical deposition from platinum solutions. Platinum nanoparticles in the size interval of 1–4 nm were prepared in this manner. Specifically, three sets of platinum nanoparticles of different sizes were prepared, namely, 1.9, 2.4, and 3.1 nm. The CO_{ads} oxidation stripping voltamograms and current–time transients for the CO_{ads} oxidation using potential step experiments were studied. It was observed that the position of the CO_{ads} stripping peak shifted to more positive values with a decrease in particle size. The experimental data for the current–time transients were compared with calculated curves. A basic model involving active sites for −OH formation was suggested. The model assumes that the active sites for the −OH formation reaction are located at the circumference of the spherical platinum nanoparticle, to which the CO_{ads} molecules diffuse and are subsequently oxidized to CO_2. According to this initial model and its correspondence with the experimental data, a restricted surface mobility of CO_{ads} on platinum nanoparticles of less than 2 nm is suggested. For the platinum nanoparticles larger than 3 nm, a transition to faster CO_{ads} mobility is reported. This work presents the theoretical treatment of experimental CO_{ads} oxidation data for nanosized catalysts. It is initial work that involves a simple model. A good fit between the theoretical and experimental data is obtained. Further testing and possible parameter adjustments of the model are needed. Obviously, data need to be added for additional catalyst particle sizes and for catalyst particles that are of narrow size distribution. Also, useful data could be obtained regarding the adsorption strength of CO and OH as a function of the particle size using complementary methods. Methods such as *in-situ* infrared (IR) spectroscopy and/or *in-situ* X-ray adsorption (XAS) are often applied for such studies. The suggested differences in the CO_{ads} mobility for the different platinum particle sizes may be explained by a dependence of the CO_{ads} bonding strength on the particle size. An estimate of a number of relevant kinetic parameters, such as the diffusion coefficient, reaction rate constants, number of active sites, etc., can be potentially obtained through the combination of theoretical and experimental data for current–time transients of the CO_{ads} oxidation reaction.

2.1.4. Measuring Activities for Nanosized Catalysts

(a) Rotating Disc Experimental Measurements and Fuel Transport to Catalyst Sites. Much effort and many discussions have focused around the understanding and origin of true intrinsic catalytic activities of nanosized catalyst particles. This is particularly interesting as the intrinsic catalytic activity applies to reaction conditions that are activation controlled. Changing from activation to mass transport controlled conditions raises the question as to whether a particle size effect should be observed for rapid charge transfer reactions such as the H_2 oxidation reaction and the O_2 reduction reaction. It also raises the question as to how intrinsic electrocatalytic activities for rapid charge transfer reactions need to be measured. One approach is the use of isolated nanoparticles, as discussed below. Rotating disc experiments (RDE) are typically employed to study reactions with elements of mass transport control and are routinely done for the orr. At low overpotentials, a reduction current independent of the rotation rate is observed, followed by a region of mixed activation and mass transport control, and eventually a limiting current that is indicative of a purely mass transport controlled reaction (see Fig. 3). Inspection of the orr data for a clean platinum bulk metal electrode [34] indicates that transport limitations become important at currents larger than -1 mA cm^{-2}. Information about the electrocatalytic activity can still be obtained using the RDE data, despite the fact that mass-transport limitations occur. The Levich-Koutecky equation is used for this case, as follows [9]:

$$\frac{1}{i} = \frac{1}{i_{ac}} + \frac{1}{i_l}$$

where

$$i_l = B\omega^{1/2} = 0.62n\mathrm{F}D^{2/3}\nu^{-1/6}\omega^{1/2}c^o$$

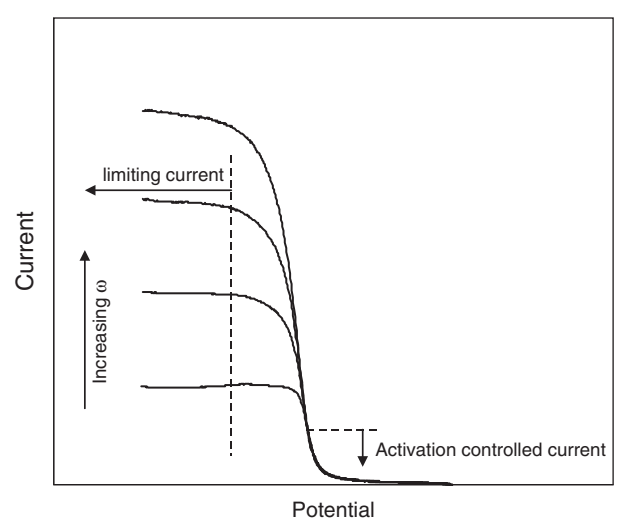

Figure 3. Examples of current–potential curves for different rotation rates (ω), showing the different regions, i.e., activation versus mass transport (limiting) current control.

In these equations, n is the number of electrons, F Faraday's constant, D the Diffusion coefficient, ν the viscosity of the electrolyte solution, ω the rotation rate, and c^o the reactant concentration. A plot of the inverse of the measured current versus $\omega^{1/2}$ gives an intercept at zero rotation rate that yields a measurement of the activation-controlled part of the reaction. This method is frequently applied to bulk metal electrodes as well as nanoparticle catalyst electrodes. One precaution needs to be taken when high surface area electrodes are used such as, e.g., supported nanoparticles. It is important that only a thin layer of catalyst is studied, as otherwise mass transport limitations into the catalyst layer rather than catalytic activities may be studied. Testing whether the electrode is sufficiently thin to allow the extraction of activation-controlled data is straightforward. First of all, it is recommended that the electroactive surface area is smaller than the geometric surface area. Second, careful inspection of the current-potential curves at low overpotentials should show that they are to be independent of the rotation rate. If these two conditions are achieved, the RDE measurements and the Levich-Koutecky equation can be employed to extract information about the intrinsic catalytic activity of nanoparticles.

The issue of a possible influence of mass transport limitation with high surface area electrodes and nanoparticles is important when experimental data are used in an attempt to extract intrinsic catalytic activities and compare different catalysts. This issue is highlighted by the "territory effect" proposed by Watanabe and Stonehart, which is suggested to be responsible for the experimentally observed influence of catalyst particle size on the orr [26]. If the reaction is studied in a range where elements of mass transport conditions influence the current, then the diffusion profiles are influenced by near-by neighboring catalyst particles, as shown in Figure 4. In this case, the number of catalyst surface sites involved in the faradaic reaction becomes a function of the particle size and dispersion (nearest neighbor distance). Hence, one may study mass transport effects rather than differences in catalytic activities as discussed by Stonehart and Watanabe. The use of well-dispersed catalysts and/or thin, i.e., low surface area, electrodes is expected to allow the measurements to take place in the activation-controlled regime that reflects true intrinsic catalytic activities. The question of mass transport limitation versus catalytic influences is of great importance for real systems. Real systems consist of three-dimensional structures within which a mix of activation and mass transport controlled regimes exits.

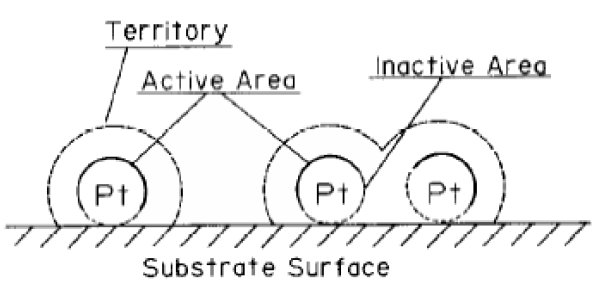

Figure 4. "Territories of supported catalyst particles relating to reactants" proposed to explain the so-called size effect in the O_2 reduction activity. Reprinted with permission from [26], M. Watanabe et al., *J. Electroanal. Chem.* 261, 375 (1989). © 1989, Elsevier Sequoia S.A., Lausanne.

(b) Single Nanoparticle Approach. The complexity of studying true electro-activities for "single" nanosized catalysts is reflected by work carried out in Stimming's research group [37, 38]. They prepared single palladium nanoparticles on Au(111) surfaces using a scanning tunneling microscope (STM) tip. For the deposition of the single nanoparticle, an approach developed by Hofmann et al. was adopted in that work [39]. Palladium, predeposited onto the STM tip, was transferred to the Au(111) substrate via a jump to contact approach. The STM tip was subsequently used to image the particle. From these images the particle shape and height were obtained, i.e., quantities which are subsequently used to estimate the surface area of the nanoparticle. Using this approach, three different sizes of palladium nanoparticles were studied, namely, isolated particles of 0.5-nm height and 6-nm diameter and single particles of 2.5-nm height and 12-nm diameter and 10-nm height and 200-nm diameter. Immediately after preparation, the STM tip was used as a probe to measure the activity of the individual particles for the H_2 oxidation reaction. Details of the experiments and measurements are given elsewhere [37, 38]. The basic principle is that H_2, which is evolved on the palladium nanoparticles under potentiostatic control, is collected on the STM tip, where the H_2 is oxidized and the oxidation current is related to the H_2 production activity of the different palladium nanoparticles. The group reported increases in the intrinsic rate constant for the H_2 evolution reaction of orders of magnitudes for palladium particles decreasing from bulk palladium metal to nanometer-sized palladium particles. There also appears to be a change in mechanism of the H_2 evolution reaction when comparing the small palladium nanoparticles on Au(111) versus a polycrystalline Pd bulk metal substrate. For the latter, a Tafel slope of 120 mV dec^{-1} is observed, while for the nanoparticle systems the Tafel slopes approach 60 mV dec^{-1} with decreasing particle size. This change may be related to alloying effects of palladium with gold. This raises the question as to whether the palladium particles are true nanoparticles and to what extent the support influences the nanoparticle properties. However, and very importantly, the results for such experiments need to be examined with care. The method of estimating the activity for the H_2 evolution reaction has raised a number of questions. Questions to the work and responses from the research group can be found in a special article of Faraday's discussion [37]. Questions regarding the capability of using an STM tip to measure the H_2 generated at a small particle roughly 300 nm away from the tip were raised and inquiries were made about the unusual profile of the experimentally observed current–time transients. Another issue that seems not to have been discussed in the literature is the possible error in obtaining the current density values for the H_2 evolution reaction of the single nanoparticles. The current values measured experimentally are very small, and a large area normalization factor is needed to compare the intrinsic activity of the nanoparticles to the of bulk palladium metal. An interesting aspect of the use of single nanoparticles for electrochemical processes and studies is the fact that the diffusion limiting current of nanoparticles is much higher than for an equivalent, flat bulk electrode. This

is seen as follows, in the equation of the diffusion limiting current density (j) for a semihemispherical particle:

$$j = nFDc_0\left(\frac{1}{\sqrt{\pi Dt}} + \frac{1}{r_0}\right)$$

where n is the number of electrons transferred, F is Faraday's constant, D is the diffusion coefficient, c_0 is the initial concentration of the reactant, and r_0 is the radius of the catalyst particle. (For a single, i.e., isolated, particle, the diffusion profiles do not overlap; hence, the above equation applies.) It is seen from this equation that the smaller the particle, i.e., the r_0 value, the more dominant is the term on the right-hand side in the j limiting equation. The benefit of nanosized particles (radius) on the limiting current density is shown in Figure 5 after 1 s, using a typical diffusion coefficient for ions in aqueous solution of 10^{-6} cm^2 s^{-1} and a concentration of 10^{-4} mol cm^{-3} and assuming a one electron reaction. Higher limiting current densities are achieved for nanoparticle electrodes, allowing the study of fast interfacial reactions over a broad potential range. The increase in the limiting current density value is roughly a thousand times when changing from an electrode of 1 cm to a 1 nm radius.

This kind of research is also extremely difficult partly because of the limited stability of the nanoparticles formed on the foreign substrate. Typically, the measurements are carried out within a few hours. The instability of nanoparticles prepared in such a manner is related to the fact that the particles have a high surface area, which is equivalent to a high surface energy, and that no effort is made to stabilize them. Such stabilization could be achieved by the deposition of the nanoparticles onto imperfections in the substrate, perhaps at kink sites, or by the use of organic stabilizers. However, one should note that a real advantage of using electrochemical methods to prepare nanoparticles is the fact that nanosized catalyst particles can be prepared without the use of stabilizers. The stabilizers themselves are not desired for heterogeneous catalysis and typically alter the catalyst properties. Distinguishing between particle size and stabilizer influences becomes difficult. Hence, nanosized catalysts prepared via electrochemical methods can potentially assist in understanding the relationship between particle size, structure, and catalytic activity. The actual size and stability of such nanoparticles is strongly dependent on the interaction energies between the nanoparticle and the substrate. This has been extensively reviewed and discussed by Budevski et al. [40].

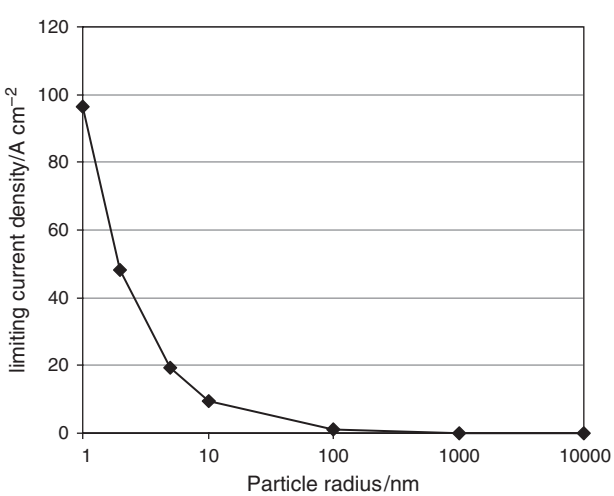

Figure 5. Calculated limiting current density (j) for a single particle as a function of the particle radius. A one electron reaction, a diffusion coefficient of 10^{-6} cm^2 s^{-1} and an initial concentration of 10^{-4} mol cm^{-3} were used for the calculation.

Electrochemistry is indeed very useful to potentially make nanosized and nanostructured catalyst systems. The power of electrochemistry as a tool to make nanostructured surfaces has been known for decades. It was shown by Budevski et al. that controlled amounts of silver can be electrodeposited in the submonolayer range on a Ag(100) substrate [41–44]. In case of strong interactions of the metal adatom (Me_{ads}) and the substrate (S), underpotential deposition (upd) occurs and can be used to grow 2D Me_{ads} phases and/or 2D Me-S surface alloys, while for weak interactions these 2D phases are not observed. The power of electrochemistry lies in its potential to, e.g., deposit metals on a foreign electrode substrate by upd and/or the utilization of the overpotential component to induce controlled nucleation of the Me_{ads} on the substrate and subsequent growth of the deposited Me_{ads} cluster. As compared to traditional chemistry routes, where the concentration, pressure, and temperature can be used to influence the properties of the products, electrochemist have an additional parameter, the overpotential (η), to utilize and make nanostructured electrode surfaces. A new crystal may be formed if the ambient phase is supersaturated (difference in the chemical potential ($\Delta\mu$) > 0). In electrodeposition, the supersaturation of the ambient phase is given by the overpotential ($\eta = E - E_{Me/Mez+} < 0$), where E is the applied potential. Hence, the application of an overpotential can result in the nucleation of small clusters that can be subsequently grown at a lower potential, where the formation of new nuclei does not take place. Particles of controlled and narrow size distribution can be made in this manner [40]. This growth mechanism of clusters of controlled size is shown in Figure 6.

This potential power of electrochemistry, i.e., to make nanostructured surfaces that are also of interest to electrocatalysis, has in particular been explored by Penner's research group. They have applied the method to a variety of systems, such as silver, gold, platinum, molybdenum, and nickel on graphite basal planes [45–47]. For this chapter, the preparation of platinum nanoparticles on basal plane oriented graphite surfaces is of interest. The Penner group used solutions of H_2PtCl_6 in HCl to reportedly deposit platinum nanoparticles of crystallite diameters of less than 4 nm onto the graphite surfaces. It was observed that platinum nucleated both at defect sites and at defect-free regions. The particle size was varied by changing the time of growth at the selected, constant overpotential. A large overpotential was selected, at which in fact not only the reduction of the platinum salt to platinum metal takes place but also the adsorption reaction of hydrogen on platinum. The particles were characterized using noncontact atomic force microscopy (AFM), a technique which accurately measures the height of the particles. Typical AFM images of platinum deposits on basal plane graphite are shown in Figure 7.

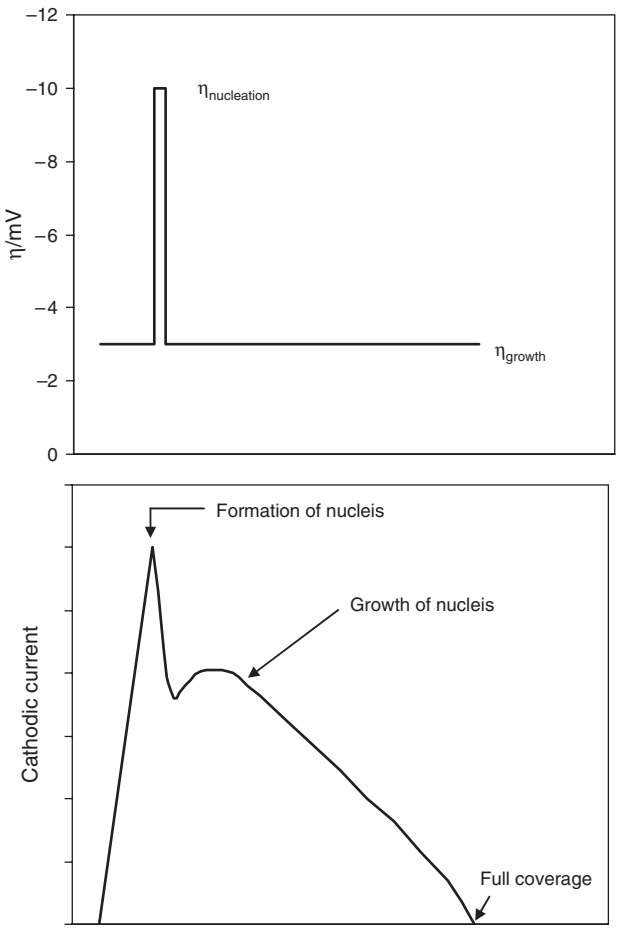

Figure 6. Schematic of potentiostatic double pulse technique used to initiate nucleation at a high overvoltage ($\eta_{nucleation}$), followed by particle growth at low overvoltage (η_{growth}). Figure 6(a) shows the scheme for the potential double pulse, while Figure 6(b) shows the expected current response in a qualitative manner.

2.2. Preparation of Nanosized Fuel Cell Catalysts

2.2.1. Requirements for Fuel Cell Catalysts

The development of optimized and improved catalysts for an effective fuel cell technology is challenging. In the case of the anode catalyst for H_2/O_2 fuel cells, which run on H_2 contaminated with CO, and CH_3OH fuel cells, the basic structure of the catalyst surface is known. In simple terms, a nanosized catalyst consisting of Pt and Ru sites that are uniformly and optimally distributed on the surface is desired. There is some discussion about the Pt to Ru atomic ratio that yields the best activity for the CH_3OH oxidation reaction, and little is known with certainty about the structure and size influence of nanosized Pt/Ru particles on the catalytic activity. Many other catalyst systems have been studied including ternary and quarternary compositions [4]. However, for the CH_3OH oxidation reaction the Pt/Ru system appears to show the best activity. In case of the H_2 fuel contaminated with CO, a few alternatives appear to exist, as discussed later in this chapter. In the design of a catalyst for fuel cells, the chemical stability of the selected

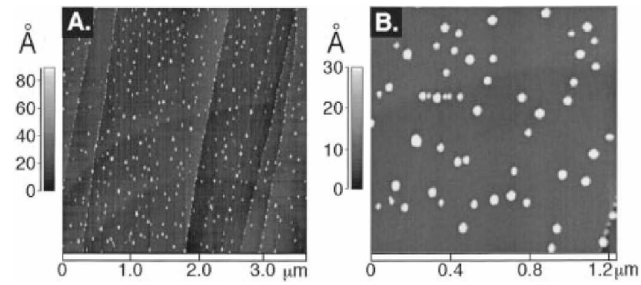

Figure 7. Noncontact atomic force microscope images, 3.4×3.4 μm (A) and 1.2×1.2 μm (B), of the graphite basal plane surface following the application of a 10 ms platinum pulse. A deposition charge of 4.84 $\mu C\,cm^{-2}$ was obtained corresponding to 0.0050 equivalent platinum atomic layers (assuming an adsorption electrovalency of 4.0). The mean particle height on this surface was 2.5 ± 0.9 nm. Reprinted with permission from [45], J. V. Zoval et al., *Phys. Chem. B* 102, 1166 (1998). © 1998, American Chemical Society.

system needs to be considered. The catalyst needs to be stable under acidic conditions, and in case of the O_2 cathode, stability at a high anodic potential is also required. There are only a few choices in the periodic table that satisfy these conditions, these being the noble metals and tungsten oxides. Mo oxides and tin are also considered stable provided that low potentials are utilized. Furthermore, the platinum and admetal or oxide sites need to be optimally distributed preferably on the atomic scale. Therefore, alloys appear to be a good choice. However, even for alloys, differences in the surface energies of the different metals and the resulting affect on the surface structure of the catalyst particle needs to be considered. An additional requirement is that the admetal (oxide) needs to be able to generate −OH species that can be utilized in the complete CO and CH_3OH oxidation reactions to CO_2 at low potentials according to the bifunctional mechanism. The possibility of the ad-metal altering the catalytic properties via electronic (also referred to as ligand) effects is also often discussed. However, the general view appears to be that the bifunctional effect of ruthenium (shift of ca. 0.3 V) is much stronger than electronic effects [2].

Based on the knowledge of reaction mechanism and particle size measurements, it appears that researchers have a good idea about the kind of catalyst desired (although further improvements of electrocatalytic activity, namely, generation of −OH species at lower potentials, is still needed). A true challenge in this area is the preparation of nanosized catalysts of controlled size and structure. However, development in this area is complicated by the fact that the thorough characterization of nanosized catalysts is a challenge in itself. In fact, the further development of characterization tools for nanosized catalysts that allow in particular the characterization of the catalyst surface on the atomic scale is strongly required.

2.2.2. Focusing on the Pt/Ru Catalyst System

(a) "Traditional" Preparation Methods of Nanosized Catalysts for Fuel Cell Reactions. The routes so far chosen for making nanosized fuel cell catalysts can be roughly divided into two groups, namely, the impregnation (a) and

the colloidal method (b). There is a vast field of literature and expertise available for the preparation of supported nanosized catalysts (including platinum based and multicomponent catalysts) from heterogeneous gas-phase catalysis. Particularly, the impregnation method has been applied and studied extensively. In this method, a suitable support (typically carbon black for PEM type fuel cell catalysts) is impregnated or ion-exchanged with precursor salts such as, e.g., $PtCl_2$, H_2PtCl_6, or $Pt(NH_3)_4Cl_2$ [49, 50]. The precursor salt is then decomposed at elevated temperatures in a reducing atmosphere. Often hydrogen is used to avoid the oxidation of the catalyst surface. This method is well-known to result in nanosized catalysts. There are, however, challenges associated with this method that can be summarized as follows:

(1) strong influence of support on resulting properties of nanosized catalysts;
(2) possible temperature induced agglomeration of catalyst particles;
(3) possible temperature induced segregation of different catalyst components.

The latter is of particular importance for the Pt/Ru system and is related to the fact that the surface energies of platinum and ruthenium have a 2 eV difference, platinum being the larger atom having a tendency for surface segregation. This results in catalyst surfaces that are enriched in platinum. The effect becomes more pronounced as the temperature is increased. In the case of unsupported PtRu alloy catalysts, it has been shown that heating in air results in Pt and Ru phase separation and changes in the PtRu alloy component [6]. The phase separation is already observed after heat treatment at temperatures just above 200°C for 1 h. Also, heating in an oxidizing atmosphere results in the formation of RuO_2 that is volatile. A number of supported Pt/Ru nanosized fuel cell catalysts have been made using higher temperature methods. Often PtRu alloy formation is claimed to have been achieved based on powder X-ray diffraction (XRD) results. However, one needs to note that XRD data for nanoparticles need to be treated with care. Furthermore, an internal standard needs to be added to the powder to ensure that sample displacement effects are not responsible for shifts in the diffraction peak position. For platinum particles of just less than 1 nm diameter, the majority (>80%) of the atoms are on the surface. Therefore, the large difference in cohesive (surface) energy between platinum and ruthenium also implies that Pt and Ru alloys cannot be formed for very small particles.

The second method, referred to as colloidal synthesis route in this chapter, involves the preparation of platinum or bimetallic platinum based colloids in solution. A method very well-known to electrochemists and used for the preparation of platinum and platinum-based multicomponent catalysts is the "Boennemann" method [50]. The method involves the dissolution of, e.g., $PtCl_2$ in a solvent and the subsequent reduction by an added reducing agent. The reaction is summarized in the following equation:

$$PtCl_2 + 2N(Oct)_4[BEt_3H] \xrightarrow{THF/Argon} Pt[N(Oct)_4Cl]_2 + 2BEt_3 + H_2$$

where $N(Oct)_4[BEt_3H]$ stands for tetraoctylammoniumtriethylhydroborate. This compound acts as stabilizer and reducing agent. The tetraoctylammonium stabilizer used in the Boennemann synthesis method is a bulky compound. Stabilization of the colloidal particle using this stabilizer takes place via steric hindrance, i.e., resulting in catalyst particles shown in the schematic of Figure 8. The colloidal catalyst particles can be deposited on various substrates and it has been shown that the bulky stabilizer can be removed by oxidative heat treatment. However, for complete removal of this particular stabilizer, temperatures of at least 300°C are needed [51]. Removal of the stabilizer is considered essential for effective heterogeneous catalysis in order to not block valuable noble metal catalyst sites and allow access of the fuel to the active catalyst sites. Unfortunately, the high temperatures needed also alter the catalyst particle properties, as discussed above. Alteration of catalyst properties is of particular concern for bi- and multimetallic systems. The Boennemann method has also been tested for the synthesis of a number of bimetallic platinum based catalysts such as Pt/Ru and Pt/Sn nanoparticles [52]. In the latter case of the Pt/Sn nanoparticles, the influence of heat treatment on the catalyst properties has been discussed. Pt/Sn nanoparticles of nominal atomic Pt:Sn composition of 3:1 and particle size 1.5 ± 0.4 nm were prepared by the coreduction of the metal salts. Tetraoctylammonium was used also as stabilizer. The Pt/Sn nanoparticles were then heat treated in He at 200°C. The heat treatment was found to result in the coalescence of neighboring particles as well as in structural changes of the Pt/Sn nanoparticles. More precisely, cubic particles of Pt:Sn atomic ratio of 80:20 atom% and of 3.1 nm particle size were identified. A minor phase of the Pt/Sn particles consisting of hexagonal and stoichiometric Pt/Sn particles of 4.4 nm size was also found. The work clearly demonstrates the influence heat treatment can have on multicomponent catalyst systems.

Other methods than the one developed by Boennemann et al. for the colloidal synthesis of platinum and platinum based nanosized catalysts have been discussed and numerous examples can be found in the literature, as further discussed below. A very attractive method appears to be the polyol synthesis method. The polyol synthesis method has been applied to the preparation of numerous high surface catalysts including non-noble metal catalysts such as nickel. The first reported use of the polyol synthesis for the

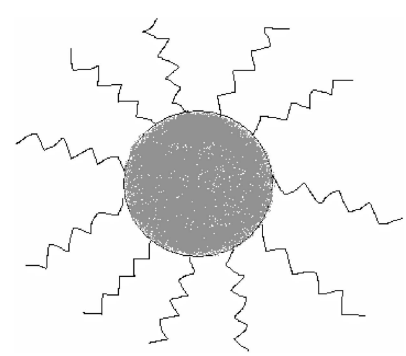

Figure 8. Schematic (not to scale) illustrating the stabilizing effect of large organic molecules on e.g., a colloidal Pt particle.

preparation of Pt/Ru catalysts for low temperature fuel cell applications appears to be a patent by Laine et al. [53]. In this method, carbon-supported and unsupported Pt/Ru catalysts are formed by dissolving the precursor salts in a polyhydroxylic alcohol (polyol) and the reduction of the noble metal precursor salts typically takes place at elevated temperatures. Preferably a viscous alcohol is used, namely, a diol, triol or tetraol. The goal is to form mixed-metal catalyst powders with particle sizes of less than 1 μm, preferably less than 0.1 μm, or less than 0.05 μm. In their work, the influence of the metal precursor salt concentration and metal loading (per weight and surface area of support) on the resulting catalyst particle size was discussed. For high metal concentrations, the reduced catalyst particles typically precipitate out off solution in the form of high surface area powders. Alternatively, colloidal solutions of, e.g., nanosized catalyst particles can be formed upon the addition of large amounts of hydroxides to the polyol (discussed for ethylene glycol) synthesis solution. The preparation of single metal, platinum, ruthenium, and rhodium colloidal solutions in ethylene glycol has been discussed by Wang et al. [54]. In that work, very small particles of 1–2 nm size and very sharp size distributions were formed. The synthesis solution was adjusted to pH 11 using NaOH, which is believed to assist in the formation of colloidal hydroxide salt formation of the individual metals tested. In recent work, the ethylene glycol method has been modified and expanded to the so-called microemulsion method and microwave synthesis [55, 56]. Pt/Ru nanoparticles supported on carbon were prepared in this manner. The ethylene glycol synthesis method has also been applied to the preparation of carbon-supported platinum catalysts, which were then tested for their fuel cell performance [57].

It has also been shown that the size of Pt/Ru nanoparticles can be adjusted using the polyol synthesis method. The composition of the resulting alloy remains the same and Pt/Ru particles between ca. 1 and 4 nm were prepared in a size-selective manner. The key to the size control is proposed to be the synthesis solution pH. In the polyol synthesis method, ethylene glycol acts as solvent as well as reducing agent for the platinum and ruthenium precursor salts [58]. The main products found for the oxidation of ethylene glycol were glycolate and some oxalate (depending on the synthesis solution pH, these species are either present as anions or in their acid form). The amount of glycolate and oxalate formed was found to be independent of the synthesis solution pH. An electron balance calculation suggested that at least 60% of the electrons needed for the reduction of platinum and ruthenium precursor salts are donated by the oxidation reaction of ethylene glycol to glycolate. It is believed that glycolate acts as stabilizer for the Pt/Ru nanoparticles. Depending on the pH, this species is present as either glycolate or as glycolic acid in the synthesis solution. The latter is suggested to have smaller interactions with the Pt/Ru nanoparticles, i.e., thus not provide a stabilizing function for the nanoparticles. Therefore, the principle mechanism of this size-controlled synthesis of Pt/Ru nanoparticles is suggested to result from different amounts of stabilizer (glycolate) produced during the synthesis. Furthermore, the fact that the rate of the reduction reaction of the precursor salts is not affected by the change in solution pH allows for the preparation of the same alloy compositions but different particle sizes by simply adjusting the synthesis solution pH. It is noteworthy that a similar principle, acid versus anion form of particle size adjustment, has been shown later [59] for the synthesis of Pt nanoparticles in ethylene glycol solutions. In that study, citrate was added as stabilizer for the nanoparticles, and the pH of the synthesis solution was adjusted to vary the ratio of the citrate anion versus the citric acid. $NaBH_4$ was used as reducing agent. It is interesting that citrate is a less favorable stabilizer than glycolate or oxalate, as temperatures as low as 160°C are insufficient to completely oxidize the stabilizer to CO_2 even in the presence of platinum. The increased difficulty of oxidizing citrate versus the smaller carboxylic acid molecules to CO_2 is also documented in standard electrochemical oxidation studies using bulk noble metal electrodes [60].

Pt/Ru particles synthesized by the polyol method can be deposited on conductive, high surface area substrates, thus allowing the formation of three-dimensional electrode structures. High loadings of these catalysts of very small particle sizes (tested for 2.5 nm Pt/Ru catalysts) and on various substrates can be achieved by adjusting (acidification) the pH of the colloidal synthesis solution. The size of the nanoparticles is not affected by the addition of acid once the nanoparticles have been formed. This could indicate strong interactions between the glycolate and the Pt/Ru nanoparticle surface. Another attractive feature of the ethylene glycol synthesis method is the simple form of the glycolate that is believed to act as stabilizer for the Pt/Ru colloids. The interactions between the glycolate and the Pt/Ru nanoparticle surface are believed to be strong; however, the decomposition of glycolate to CO_2 is catalyzed by platinum and takes place at "low" temperatures. In fact, the glycolate can be removed from the Pt/Ru nanoparticle surface at temperatures as low as 160°C, this temperature being sufficiently low to avoid temperature-induced modification of the Pt/Ru nanosized catalysts. The stability of the colloidal Pt/Ru ethylene glycol solution is not known with certainty and to the best of our knowledge has not been carefully investigated. While it is possible that particle agglomeration takes place in the solution, the stability of the Pt/Ru nanosized catalysts supported on, e.g., high surface area is very high (at least longer than 2 years). Also, the particle size is independent of the catalyst loading on the carbon support and independent of the support material. This makes it possible to systematically study the influence of support, particle size, and particle composition on catalytic activities.

A challenge other than the systematic control of size of bimetallic catalysts is the preparation of PtRu catalysts (likely also other bimetallic Pt based catalysts) with a high degree of alloying, i.e., the dissolution of "high" amounts (desirably up to 30–50 atom%) of Ru in the Pt face centered cubic lattice. This is in fact also a challenge for unsupported Pt/Ru catalysts [58]. It has been shown that a key to making Pt/Ru catalysts of a high degree of alloying is the very rapid and simultaneous reduction of the platinum and ruthenium precursor salts [6]. Pt chlorides are relatively rapidly reduced, while the reduction of the Ru chloride is slower. Both reaction rates can be enhanced by adding a large excess of a strong reducing agent (e.g., $NaBH_4$) very rapidly to the precursor salt solution. This concept has been explored for

the synthesis of unsupported high surface area Pt/Ru powder catalysts. It was shown that the PtRu alloy content could indeed be adjusted and unsupported PtRu alloy powders of greater than 40 atom% Ru were prepared in this manner [6]. Similar principles should be applicable to the preparation of other nanoparticles.

(b) Additional Synthesis Routes, Properties and the Characterization of Nanosized Platinum and Ruthenium Catalysts. The focus is placed on chemical synthesis methods as well as a few examples using the impregnation method followed by subsequent thermal decomposition. The examples presented in this chapter are selected, as they highlight the influence of the synthesis procedure on the properties of nanosized Pt/Ru catalysts. In some examples, the very important question of the composition of the nanosized catalyst surface structure is also discussed. Other methods very commonly used to prepare nanosized catalysts such as microwave synthesis [57], vapor deposition [61], sputter-deposition, and ball-milling [62, 63] are not discussed here. Chemical synthesis routes are very attractive, as they are in general easy to scale up, thus being practical from a scale-up viewpoint.

Nashner et al. discussed the preparation and structural characterization of carbon-supported Pt/Ru nanoparticles in 1997 [64]. Bimetallic particles of narrow size and compositional distributions were prepared. A bimetallic, neutral molecular carbonyl precursor, $PtRu_5(CO)_{16}$, was used for the preparation of the carbon-supported nanoparticles. The $PtRu_5(CO)_{16}$ precursor compound was synthesized following methods available in the literature and dispersed onto carbon black (Vulcan XC-72). Relatively small amounts of the precursor (1–2 wt% Pt + Ru) were loaded onto the carbon. The bimetallic particles were obtained by the reduction of the precursor in hydrogen at 400°C. The nanoparticles were characterized using X-ray absorption fine structure spectroscopy (EXAFS), scanning transmission electron microscopy, microprobe energy-dispersive X-ray analysis, and electron microdiffraction. A Pt:Ru atomic ratio of 1:5, i.e., the same as the bimetallic precursor, was estimated. The particle diameter was 1.5 nm and a face centered cubic (fcc) structure was found. For bulk PtRu alloys of Pt to Ru ratio of 1:5, i.e., high Ru concentration, a hexagonal close-packed structure is expected. However, this structure was not observed and this fact does not appear to be related to the nanosize of the PtRu particles (see below, synthesis and characterization work by Dassenoy et al.). It might be related to the "high" temperature used for the synthesis of the nanoparticles in the work being discussed here. In a later paper, the group reported [65] that preferential surface segregation of the platinum within the bimetallic particles takes place. It is assumed that this behavior is due to temperature-induced surface segregation of the larger platinum atoms, as expected for the Pt/Ru system. This was indicated by *in-situ* X-ray absorption studies that suggest the presence of a core–shell inversion during the growth process between 200 and 400°C. At 200°C, the platinum was found preferentially at the core of the condensing particle, while at 400°C, the nanoparticles adopted an inverted structure in which platinum is preferentially located at the surface. The synthesized Pt/Ru particles show nonstatistical distribution of the two elements. In an O_2 atmosphere, an outer metal oxide layer was formed that surrounded a metal-only core. This oxidation process was found to be reversible by exposing the particles to H_2 at room temperature. It was reported that the initial particle structure was recovered.

In a later study, Pan et al. [66] synthesized bimetallic Pt/Ru nanoparticles starting from single metal precursors, namely, $Pt(dba)_2$, where dba = dibenzylidene acetone, and Ru(COD)(COT), where COD = 1-cyclooctadiene and COT = 1,3,5-cyclooctatriene. Poly(vinyl-2-pyrrolidine) (PVP) was used as stabilizer. Bimetallic nanoparticles were formed, reducing various ratios of the Pt and Ru precursors with H_2 in tetrahydrofuran (THF) solutions. The decomposition reaction takes place at low temperatures, room temperature and less. The synthesis of single Pt [67] and Ru [68] particles via this route was described in previous work. There it was shown that fcc platinum particles and hexagonal ruthenium particles with mean particle size of 1.2–1.6 nm and 1.2 nm, respectively, were formed. The platinum nanoparticle was modeled as a closed-shell cubooctahedron. For both cases, a contraction of the metal–metal distance for the nanoparticle versus the bulk metal was observed, as follows: for platinum, 0.274 versus 0.2774 nm and, for ruthenium, 0.266 versus 0.270 58 nm. Monodispersed particles (Pt to Ru ratio of 1:3) of very small size (ca. 1.1 nm) were made that are suggested to be truncated twinned octahedrons of 79 atoms. Furthermore, a composition-induced structural change was observed for the bimetallic nanoparticles. For low ruthenium concentrations, the nanosized particles showed a fcc structure, while at high ruthenium concentrations the lattice structure changed to hexagonal closed packed (hcp).

Very recently, Harada et al. [69] also used PVP as a stabilizer to prepare a Pt–Ru colloidal dispersions. In this study, PVP was used as stabilizer, as large polymer stabilizers are known to form so-called "naked" metal clusters, meaning that strong metal–polymer interactions dominate the metal–support interactions. Therefore, these catalysts are believed to be interesting for compositional studies, i.e., the "naked" clusters are believed to be more likely to show thermodynamically equilibrium shapes (cubooctahedral in the case of platinum) and perhaps the formation of clusters with more magical numbers than particles that are strongly influenced by support interactions. Simple single metal precursor salts, namely, hexachloroplatinic acid and ruthenium chloride, were used in this study. Furthermore, a mixture of ethanol and water was used as solvent. The colloidal solution was formed by refluxing at 100°C for 2 h in air or nitrogen. Electronic spectra, EXAFS, and high-resolution microprobe analyses suggest that no PtRu alloys but rather small monoatomic platinum and ruthenium clusters are formed independent of the Pt to Ru ratio. The particle size was observed to be dependent on the platinum and ruthenium ratio. It is also suggested that clusters with the magical number of 147 could be made.

The structure and size of nanoparticles is sensitive to the synthesis method. In the case of platinum nanoparticles, it has been reported that the nature of the ligand can change the structure as well as the size of the particle. Rodriguez et al. [29] prepared fcc platinum nanoparticles of large size dispersity (1–2 nm). The particles were prepared by the reaction of $Pt(dba)_2$ with CO in toluene, which resulted in a

brown precipitate that was, after isolation, redissolved in CH_2Cl_2 to yield the colloidal solution of fcc platinum. These platinum colloids were further dissolved in THF, which led to 1.2-nm fcc platinum particles. The latter were stable and could be isolated and characterized using HRTEM and wide-angle X-ray scattering (WAXS). A new platinum colloid was formed upon the addition of triphenylphosphine (PPh_3) to the THF solution. Addition of small amounts of PPh_3 (0.2 equiv) yielded a platinum colloid of 1.2 nm, however, of icosahedral structure, while upon the addition of an excess amount of PPh_3, larger platinum colloids of 1.7 nm and of fcc structure were formed. The work focused on the structural characterization of the prepared colloids and nanoparticles, highlighting the importance of synthesis procedure and parameters on the final structure and size of the nanoparticles. A detailed discussion regarding the possible reasons for a change in the structure of the platinum nanoparticles upon the addition of different amounts of the same stabilizer was not undertaken in this study. Other factors likely influencing the structure, surface properties, and distribution of the platinum versus ruthenium atoms in nanoparticles, other than the ligand and temperature, are the reducing agent. In case of, e.g., the Boennemann method, borohydrides are used as reducing agents that may show strong interactions with the catalyst surface and perhaps form an electrically charged surface.

Dassenay et al. [70] prepared nanosized Pt/Ru particles by the decomposition of the $Pt(dba)_2$ and Ru(COD)(COT) precursors in the presence of a stabilizing polymer, namely, PVP. The precursors were dissolved in THF and decomposition and reduction took place under H_2 at room temperature. Particles of varying Pt to Ru ratio from zero to one were formed and characterized using HRTEM and WAXS. WAXS provides a set of accurate interatomic distance data and was used in this work in conjunction with HRTEM to probe the influence of the size and composition on the atomic organization and structure of the platinum- and ruthenium-based nanoparticles. Consistent with other studies, it was found that platinum crystallizes in the fcc structure and ruthenium in the hexagonal close packed (hcp) structure, i.e., the same as found for the bulk metals. Independent of the composition, the nanoparticles were found to be crystalline, which also seems to be generally observed. The WAXS investigation suggested changes in the cell parameter due to the reduction in particle size. In case of pure ruthenium, 1.1-nm diameter particles were formed and analyses of the WAXS data suggested a contraction in the *a* parameter by 1.1% (0.266 vs. 0.270 58 nm for bulk Ru), while a dilation of the *c* parameter of 1.85% (0.436 vs. 0.428 11 nm) was observed for a 100 atom ruthenium cluster. In case of pure platinum, 1.6-nm diameter particles were formed and a 147 atom platinum cluster model, in conjunction with the WAXS data, suggested a decrease in the metal–metal bond to 0.274 nm, corresponding to a compressive strain of 1.2% of the lattice parameter. It is noteworthy that 147 is a magical number for metal clusters of cubooctahedral shape [69]. In that study, a decrease in the metal–metal bond length with increasing ruthenium content was observed, from 0.274 to 0.267 nm for pure platinum to pure ruthenium. Furthermore, the frequency of the CO stretch (from gaseous CO) was found to shift to lower values with an increase in the ruthenium content, from 2043 to 2013 cm^{-1} for pure platinum to pure ruthenium. This decrease in frequency reflects an increase in adsorption strength of CO on the nanoparticle surfaces with an increase in the ruthenium content. The results were interpreted to be due to changes in the overall surface electron density in each particle, as PtRu alloys of higher ruthenium concentrations are said to be formed. Based on the evaluation of the WAXS data, a phase diagram was designed for the PtRu nanoparticles that are suggested to be disordered alloys, see Figure 9. The diagram showing the metal–metal distance as a function of the atomic ruthenium content was compared to data for bulk PtRu alloys. This is probably the first report of a phase diagram for disordered alloy PtRu nanoparticles. A shorter metal–metal distance for the Pt/Ru nanoparticles versus bulk PtRu alloys is observed. However, it appears that the structural dimensions of the Pt/Ru particles synthesized in this work are similar to those of the bulk alloys, despite their nanometer size. Another important finding of this study was the observation of an increase in twinned particles with increase in the ruthenium content. An HRTEM image of a Pt/Ru nanoparticle stabilized with PVP, showing a twinned structure, is shown in Figure 10. This appears to be another indication of the formation of alloys. The pure platinum nanoparticles stabilized with PVP display a cubo-octahedral geometry with neat (111) and (100) facets, Figure 11. They do not display twin structures.

(c) Preparation and Properties of Nanosized Model Catalysts on Single Crystal Electrodes. The use of chemical synthesis routes for the preparation of practical catalyst systems is very desirable, as they are in general easy to scale up, and, in the case of the "ethylene-glycol" synthesis method, they are safe and "inexpensive," except for the noble metal precursor salts. However, in some cases (particularly for fundamental studies) it is desirable to produce model catalyst systems that are well-characterized and defined. Such model systems typically consist of one metal and or metal oxide deposited on a conductive foreign bulk substrate. Scanning tunneling microscopy (STM) is an extremely useful tool to characterize the morphology of the nanostructure catalyst systems. In order to use STM, well-defined substrates with

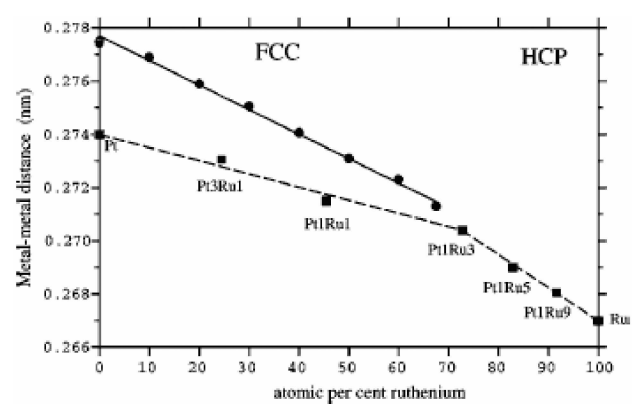

Figure 9. Evolution of the metal–metal distance with the Ru content both in our particles (dashed line) and in the fcc phase domain in the bulk alloy (solid line). Reprinted with permission from [70], F. Dassenoy et al., *J. Phys. Rev. B* 63, 5407 (2001). © 2001, American Physical Society.

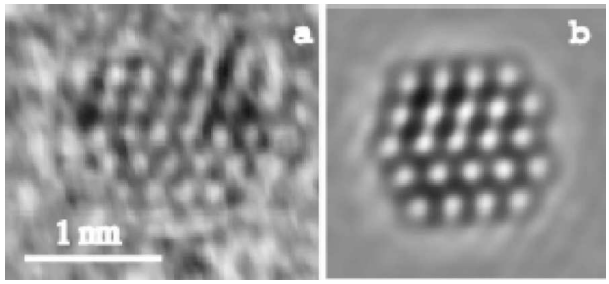

Figure 10. HRTEM micrographs and associated diffractograms of a typical Pt particle (left) and a typical Ru particle (right), respectively, observed along a fcc [011] and a hcp [$2\bar{1}\bar{1}0$] zone axes. Reprinted with permission from [70], F. Dassenoy et al., *J. Phys. Rev. B* 63, 5407 (2001). © 2001, American Physical Society.

an atomically smooth surface are needed, i.e., single crystal electrodes are generally used. Well-defined model catalyst systems can be used to study the influence of the nanosize and distribution of the admetal on an electrochemical oxidation reaction and/or the shape influence of catalyst particles and adcomponent on the reaction. The methods available for the preparation of such systems are limited. High-vacuum techniques such as sputter deposition can be used to prepare nanoparticles if the conditions are carefully tuned and controlled, while electrochemical methods can potentially provide simpler and more powerful routes for the preparation of model catalyst systems.

An interesting approach was taken by a research group in Brookhaven in an attempt to lower the Pt loading of nanosized catalysts for lower temperature fuel cells. In a series of papers [71–76], they describe their approaches to nanostructure using various conductive surfaces with Pt in the monolayer range. Initial studies were carried out using single-crystal substrates and the research was subsequently expanded to decorate nanosized substrates supported on carbon with Pt in the monolayer range. The goal was to grow two-dimensional (2-D) films of Pt. Two

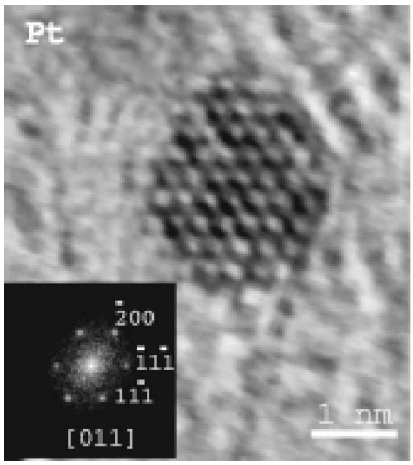

Figure 11. Comparison between (a) the experimental HRTEM image of a twinned particle and (b) the simulated image of the twinned truncuated octahedron model. Reprinted with permission from [70], F. Dassenoy et al., *J. Phys. Rev. B* 63, 5407 (2001). © 2001, American Physical Society.

approaches were used to nanostructure the surfaces with Pt. One approach was a two-step process that involved the underpotential deposition (upd) of copper and the subsequent replacement of the Cu upd with platinum [71]. The second approach explored the spontaneous deposition of platinum from Pt(+IV) chloride precursor salt solutions onto the substrates. The prepared nanostructured catalyst systems were tested for the O_2 reduction reaction and the oxidation of H_2 in the presence of CO. Platinum was deposited on a range of substrates, which, however, exclusively belonged to the group of platinum metals. The first studies were carried out using Au(111) surfaces. The two-stage method involving Cu upd was explored. First, a monolayer of Cu was formed by upd. The Cu was subsequently replaced at open circuit with either Pt, Pd, or Ag by spontaneous deposition. The driving force for the Cu replacement is the positive difference between the equilibrium potential of the noble metal and the equilibrium potential of the upd Cu adlayer on the metal substrate. In case of the spontaneous deposition of Pt from H_2PtCl_6 solutions, the reaction mechanism takes place as follows:

$$2Cu^0/Au(111) + PtCl_6^{2-} \leftrightarrow Pt^0/Au(111) + 2Cu^{2+} + 6Cl^-$$

The reduction of the Pt(IV) precursor to Pt^0 requires the oxidation of two Cu^0 atoms to Cu^{2+}. Therefore, a maximum of half a monolayer of Pt metal can be deposited onto the gold substrate using this precursor salt. STM imaging of the Pt deposits on Au(111) showed that less than a monolayer of platinum was formed, and that the platinum was deposited as a fine structure consisting of nanoclusters and nanovoids. The STM tip resolved Pt clusters of 3–5 nm size and suggested they were monoatomic in height. The deposition of Pd and Ag onto Au(111) was also tested in this manner. $PdCl_2$ and AgCl were used as precursor salts for this study. In case of the Pd(II) precursor, the oxidation of one Cu is required per Pd atom, and, hence, the deposition of a monolayer of Pd is expected, while in case of the Ag(I) surface, only half a Cu atom is needed to be oxidized per silver atom and the deposition of two monolayers of silver is expected. STM images of the two surfaces indeed support the expectations. In case of the Pd/Au(111) system, the surface is almost entirely covered with a Pd film and only a few and small parts of the gold substrate are exposed. The gold substrate is entirely covered for the Ag/Au(111) system; however, the STM studies reveal little holes in the surface structures that were measured to be one atomic layer in height. These studies demonstrate that simple methods can be used to form nanostructured films on a foreign substrate via the Cu upd method. The oxidation state of the noble metal precursor salt can be potentially used to modify the height and coverage of film growth. The substrate, however, needs to be sufficiently noble so that it is not dissolved during the spontaneous deposition process.

The second method of spontaneous deposition of platinum directly onto substrates such as Ru and Pd was also tested by this group [72–77]. In this case, the deposition of Pt takes place on a noble metal directly, i.e., without the assistance of a Cu upd layer. The mechanism and driving force for the spontaneous deposition of a noble metal onto a noble metal is not yet entirely clear. It has been suggested

that in the case of Ru, Ru surface sites may be oxidized to, e.g., RuOH. The group reported that the formation of sub- and monolayers of Pt on various noble metal surfaces is possible. The structure of the Pt deposits was found to strongly depend on the concentration of the Pt precursor salt solution. For lower concentrations, namely, 10^{-4} M $PtCl_6^{2-}$ in 0.1 M H_2SO_4, the Ru surface was covered to ca. 35% with Pt nanoparticles of columnar shape. The particles were 3–5 nm (10–15 monolayers) high and had an average diameter of 6–10 nm. Pt particles of 2–3 monolayer height and 2–6 nm diameter were formed when higher concentrations, 10^{-2} M $PtCl_6^{2-}$, were used. The surface coverage appeared to be much higher than 35% for the latter. Electrochemical studies were carried out using these catalysts and the group concluded that these catalysts, consisting of spontaneously formed platinum on ruthenium surfaces, show promising activities for the O_2 reduction reaction and the oxidation of H_2 in the presence of CO [73–77].

Kuk et al. [79] adopted the approach of the Brookhaven group to decorate commercial Ru nanoparticles supported on carbon (Ru/C) with Pt. After deposition of the platinum, the catalysts were reduced in a H_2 atmosphere at room temperature. The use of higher temperatures was found to result in particle growth. The platinum-decorated Ru/C system was tested for the electrochemical oxidation reaction of CH_3OH. For "optimized" platinum decorated Ru/C catalysts, higher activities per noble metal weight as well as per catalyst surface area were found than for the carbon-supported Pt/Ru catalyst supplied by E-tek, while all platinum-decorated Ru/C catalysts showed a lower CH_3OH oxidation activity than a catalyst obtained from Johnson Matthey. The CH_3OH oxidation activity per catalyst weight of the Johnson Matthey catalyst was ca. 4 times larger than for the platinum-decorated Ru/C system.

Other studies involved the preparation of two-dimensional, nanosized ruthenium islands on single-crystal platinum, typically Pt(111) [79–82]. The size and distribution of the deposited particles were studied as a function of the ruthenium coverage using STM [79, 81], and oxidation states of the deposited ruthenium were obtained by XPS [80]. These deposits were mainly one atomic layer in height; hence, XPS measurements reflect the entire ruthenium nanoparticle. This well-characterized systems were then used for various studies, e.g., obtaining the electrooxidation activities for CH_3OH, CO_{ads}, etc. The first studies were reported by Stimming's group, who deposited ruthenium onto Pt(111) using electrodeposition [79]. The two-dimensional ruthenium islands were deposited under constant potential control from $RuCl_3$ dissolved in H_2SO_4. Relatively long deposition periods (5 min and longer) were used. Ruthenium particles of broad size distribution (2–6 nm) were made in this manner. The particle size was found to be independent of the Ru coverage. In subsequent studies, Wieckowski's research group reported the spontaneous deposition of two-dimensional ruthenium nanoparticles on Pt(111) from $RuCl_3$ solutions in $HClO_4$ [80, 81]. The open-circuit potential for the spontaneous deposition process is roughly 0.8 V versus RHE, i.e., within the same range as used by Stimming's group for some of the electrodeposition reactions. The spontaneous deposition of two-dimensional ruthenium islands has been postulated to take place, according to the following equations. It is proposed [82] that hydrated Ru(IV) complexes are needed for the successful spontaneous deposition of the ruthenium nanoislands:

$$[RuO(H_2O)_4]^{2+} \rightarrow RuO_{2ads} + 3H_2O + 2H^+$$

$$RuO_{2ads} + 2H^+ + 2e^- \rightarrow RuO_{ads} + H_2O$$

$$[RuO(H_2O)_4]^{2+} + A^- + e^- \rightarrow RuO_{ads} + A_{ads} + 4H_2O$$

where A^- is a solution anion. Nanoislands of RuO_{ads} on Pt(111) can be reduced to ruthenium metal at low potentials [82].

The surface oxidation of platinum has been suggested as a possible complementary reaction:

$$Pt + xH_2O \rightarrow PtO_xH_y + (2-y)H^+ + (2x-y)e^-$$

Essentially very similar two-dimensional nanosized ruthenium islands were formed on Pt(111) by the two groups. In both cases, ruthenium islands of particle sizes in the 2–6 nm range, independent of the coverage, were found. The major difference between the systems obtained using the two different methods appears to be the oxidation state of the as-deposited ruthenium nanoparticles. The Illinois group reports the particles to consist of mainly Ru metal and RuO_2, while the Stimming group reports them to deposit as ruthenium metal, i.e., according to a three-electron reaction, as one probably expects. So-called *in-situ* X-ray photon spectroscopy (XPS) studies, i.e., studies in which the electrode is transferred from the electrochemical cell through a specially designed chamber into the XPS chamber, were undertaken by the Illinois group. They reported that the RuO_2 present in the nanosized ruthenium particles on the Pt(111) surface was reduced to ruthenium metal at sufficiently low potentials. The electrochemical reduction of RuO_2 present in a ruthenium nanoparticle on Pt(111) surfaces is different from the electrochemical reduction of bulk RuO_2. The latter is not electrochemically reduced to Ru metal. This difference between the nanoparticle and the bulk oxide system could be due to the fact that in the former the RuO_2 sites are located near platinum sites. This is a remarkable result that likely suggests that RuO_2 sites located near platinum sites can be reduced. This may take place by a hydrogen spillover reaction mechanism. The electrochemical reduction of RuO_2 sites near platinum has been confirmed by a later study involving a different method than *in-situ* XPS. The results are also of significant importance for the CH_3OH electrooxidation reactions. They strongly indicate that once a good distribution of ruthenium and platinum surface sites on the nanoscale range is obtained, the as-prepared oxidation state of the ruthenium should not influence the CH_3OH electrooxidation activity, as in fact the ruthenium is present in the same form once utilized under conditions relevant for fuel cell anodes.

Ruthenium nanoparticle on Pt(111) systems have been used to study the CO_{ads} oxidation characteristics. An interesting result was reported by the Stimming group [79], who used *in-situ* Fourier transform infrared (FTIR) spectroscopy for the CO_{ads} oxidation study and combined current transients recorded at a constant potential. One of their model

electrode systems with a ruthenium coverage of ca. 25% was used. In such a system, the ruthenium nanoparticles are separated by ca. 4 nm. The FTIR experiments showed that the CO adsorbed on both the ruthenium and platinum sites was completely removed at low potentials. These results likely suggest that CO adsorbed on platinum sites can diffuse across the surface to a site active for the −OH formation reaction. A CO_{ads} diffusion coefficient of $\geq 4 \times 10^{-14}$ $cm^2 s^{-1}$ was obtained for Pt(111) surfaces as the lowest potential limit, i.e., at 0.45 V versus RHE.

Wieckowski's group in Illinois also applied the spontaneous deposition route to systems other than Ru on Pt(111). Deposition of Os and Pd was tested, as well as different substrates, namely, Au(111), Pt(110), and platinum nanoparticles supported on carbon [83, 84].

(d) Surface Structures and CH_3OH Activity Influence: Ru Nanoparticles on Pt(111) versus PtRu Alloys. The CH_3OH oxidation activities for different coverages of ruthenium nanoparticles on Pt(111) were obtained for the above-discussed systems [81]. The highest activity was found for a ruthenium coverage of 20% on Pt(111). The CH_3OH oxidation activities can be compared to data published in the literature for PtRu alloys [85]. It appears that the CH_3OH oxidation activities for the spontaneously deposited nanoparticles on Pt(111) are somewhat smaller (roughly by a factor of 4) than for PtRu alloys. This could suggest that the surface structure of the alloys is more optimized than that of the 2–6 nm ruthenium islands on Pt(111). The CH_3OH oxidation activities for the ruthenium particles (formed by spontaneous deposition) is slightly higher than for 5–10 nm ruthenium islands of deposited onto Pt(111) using a ultra-high-vacuum method. This indicates the important role of the ruthenium island size and optimal platinum to ruthenium surface site distribution. Sites within the ruthenium islands are not active for large ruthenium islands, while the diffusion of adsorbed CH_3OH to the ruthenium islands takes too long if the separation between the islands is too large.

(e) Do Alloy and Nanosized Catalyst Provide Magically Different Properties Than Nanostructured Bimetallic and Bulk Metal Catalysts? The question is often raised as to how the surface of alloy catalysts looks, and there are suggestions that alloying modifies the catalytic properties. Alloys are basically not magically different from the individual metals. Inside the catalyst particles of a true alloy, one metal is dissolved in the phase of the other and a random (on the atomic level) distribution of the two metals is achieved. The structure on the surface will look different from the inside. In general, the metal with the larger size will segregate to the surface, as this gives the lowest energy state for the system. The elemental composition of the surface will thus be quite different from the bulk, with significant implications for catalytic processes. The sites on the surface behave like the single metal in the sense that they may form an oxide or dissolve. Comparing CH_3OH oxidation activity data with nanostructured ruthenium particles on bulk platinum (single crystal), it seems that the Pt/Ru alloys consist of a nanostructured surface that in terms of platinum to ruthenium site distribution is at least equivalent to the ruthenium nanoparticle system of 2–6 nm in size and a nearest neighbor distance between the ruthenium islands of ca. 4 nm on bulk platinum. The same principles for the surface versus the bulk structure basically apply for nanosized catalysts, the difference being that the surface atoms of a nanosized catalysts dominate the particle properties. Moreover, the surface structure is determined by the nanosize, i.e., the surface energy, and effects such as curvatures and particle shapes can influence the catalytic properties of the structure-sensitive reaction. The influence of many of these effects on the electrocatalytic activity of these nanoparticles has not yet been quantified. However, progress is being made in the synthesis and structural characterization of platinum-based nanoparticles, which will lead to a much deeper understanding of the catalyst structure and activity relationship. In the case of platinum-only catalyst systems, one difference is the clearly observed influence of whether the catalyst is bulk platinum metal or high surface area powders and nanoparticles. This appears as a lower overpotential for the CH_3OH electrooxidation reaction for the powders and nanoparticles. It is suggested in this chapter that this beneficial lowering of the overpotential is likely related to the bifunctional mechanism, i.e., it is assumed that the formation of –OH species is favored at, e.g., edge, kink, and defect sites of the very rough surface of the platinum powders. Interestingly, this effect appears to not be observed to nearly the same extent for the CH_3OH oxidation reaction of bulk metal PtRu alloys versus PtRu alloy powders.

2.3. "Alternative" Bi- and Multimetallic Nanosized Platinum-Based Catalysts

A large variety of catalysts other than Pt/Ru have been tested as potential candidates for the CH_3OH oxidation reactions. Gold nanoparticles have attracted a considerable amount of attention, and the electrocatalysis reactions to potentially use alternative fuels, other than CH_3OH, have also been studied extensively [86–88]. A large number of studies, particularly for gold nanoparticles, discuss reactions for the case of alkaline solutions. The influence of solution pH is indeed important for the electrocatalysis reaction and sometimes higher reaction rates than in acid solutions are observed. However, caution needs to be taken and not just reaction rates, but also the reaction mechanism and reaction products, need to be identified. The mechanism of the electrooxidation reaction for methanol and other alcohols such as ethanol and ethylene glycol, frequently suggested as alternative fuels, is pH dependent. Alcohols are weak acids, for example CH_3OH has a pK_a of ca. 15. Therefore, in an alkaline solution of, e.g., pH 14, methanol is present at about 10% in its depronated form, namely CH_3O^-. This species interacts differently with the catalyst surface than CH_3OH, namely, with the oxygen rather than the hydrogen end attracted to the catalyst surface. This results in undesired oxidation products and not CO_2, as in acidic solution at low potentials. It should be noted that even at a lower pH of, e.g., 12, there will still be a significant fraction, ca. 0.1%, of the methanol present in its depronated form, enough to react with the surface and shift the reaction equilibrium. For the development of effective catalysts for methanol fuel cells, studies in acidic solutions are hence essential. Therefore, detailed work carried out discussing the electrocatalysis for nanosized catalysts in alkaline solutions is not included in this chapter. Another issue of practical importance that also

needs to be considered when the solution pH is selected is the fact that in alkaline solutions carbonate instead of CO_2 is formed. The carbonate can cause operational problems as it could clog tubes, pumps, etc.

2.3.1. Os

A number of catalyst and nanosized catalyst compositions other than Pt and Pt-Ru have been tested for the CH_3OH and CO_{ads} and CO oxidation reactions. In the case of CH_3OH oxidation, it can be said that Pt/Ru catalysts generally show the best activities. Some studies report that Pt/Os based catalysts show comparable, but not better, catalytic activities compared to optimized Pt/Ru catalysts [90]. Considering the high toxicity of Os, one has to rule out its possible use in any practical application. Nevertheless, from a fundamental viewpoint, the investigation of Pt/Os catalysts and their structure–catalytic activity relationship is of interest. It is important that true (intrinsic) catalytic activities for a particular reactions and catalysts are measured in order to understand the relevant factors needed for a successful development of catalysts.

2.3.2. Tungsten and Molybdenum Oxides: H-Spillover Mechanism?

The importance of comparing true catalytic activities for different catalysts has been discussed in detail for the CH_3OH oxidation reaction using the nanosized Pt, Pt-Ru, Pt-WO_x, and Pt-Ru-WO_x catalysts supported on carbon black [91]. In many publications, the addition of tungsten oxide or tungsten bronze to platinum is claimed to improve the catalytic activity of these catalysts for the CH_3OH (and in some cases also for the CO) oxidation reaction [92–94]. A so-called hydrogen spillover model, first proposed by Shen and Tseung, has been proposed to be responsible for the apparent catalytic enhancement [92]. The proposed mechanism involves the continuous formation and oxidation of tungsten bronze, as follows:

(a) Formation of tungsten bronze:

$$WO_3 + x\mathrm{Pt} - \mathrm{H} \rightarrow \mathrm{H}_x\mathrm{WO}_3 + x\mathrm{Pt}$$

(b) Oxidation of the tungsten bronze:

$$\mathrm{H}_x\mathrm{WO}_3 \rightarrow x\mathrm{H}^+ + x\mathrm{e}^- + \mathrm{WO}_3$$

In this proposed reaction scheme, the CH_3OH adsorbs on the platinum surface, followed by dehydrogenation of the adsorbed species, resulting in Pt-H. The role of the WO_3 is to keep the Pt sites clean by the formation of tungsten bronze (H_xWO_3). Similar to the bifunctional mechanism, where the catalytic advantage is believed to result from the formation of OH species adsorbed at the admetal (typically Ru) of a bimetallic catalyst, the distribution of the Pt to WO_x sites on a very homogenous and fine scale is important in establishing the degree of activity. Unlike Pt/Ru systems, Pt/WO_x does not form alloys and a good distribution between the Pt and WO_x catalyst sites may not be the case, i.e., the actual number of neighboring platinum to WO_x sites may be small. Therefore, one may expect the number of H-spillover reactions from platinum to WO_x sites to be small. This has been pointed out for the carbon-supported Pt-WO_x and Pt-Ru-WO_x catalysts by Yang et al. [91]. In that work, it was shown that higher mass activities for nanosized Pt-based catalysts containing WO_x could be achieved as compared to the equivalent WO_x free catalysts. However, the true (intrinsic) catalytic activity for the CH_3OH electrooxidation reaction is essentially the same for WO_x containing versus WO_x-free catalysts. The addition of metal oxides such as tungsten oxides may, however, provide a beneficial effect on the electrocatalysts in other ways than via true catalytic promotional effects. The addition of metal oxides may e.g., avoid the agglomeration of the nanosized catalyst particles during electrochemical operation.

There are a number of papers that report a beneficial effect with the addition of molybdenum to Pt catalysts for the CH_3OH electrooxidation reaction [95, 96]. Molybdenum is present as molybdenum oxide and similar to the WO_3/H_xWO_3 system, a H-spillover mechanism has been suggested to explain the apparent beneficial catalytic activity of the Mo oxide. The reported conclusions about the catalytic activity of the Mo oxide for the CH_3OH electrooxidation reaction are based on measured currents at a particular potential and are typically not normalized for the real electroactive Pt area. Closer inspection of the CH_3OH electrooxidation onset potential from cyclic voltammetry data suggests the values to be essentially the same as for polycrystalline Pt only catalysts. To the best of our knowledge, there is only one report that shows CH_3OH electrooxidation activities at lower potentials for a Pt/Mo oxide versus Pt-only catalysts supported on carbon black [96]. Complete catalyst characterization would be useful in understanding the reported effect, and additional confirmation experiments would be beneficial.

2.3.3. Sn

The Pt/Sn system has received much attention due to the fact that Pt/Sn catalysts exhibit catalytic activities for the electrooxidation of CO, while the reports for CH_3OH oxidation are contradictory. Wang et al. pointed out that work reporting the beneficial catalytic CH_3OH electrooxidation at Pt/Sn catalysts is for nonalloyed catalysts [97]. They prepared PtSn alloys by sputter deposition that have better stability in acidic solutions and they found that the PtSn alloys do not show an enhanced CH_3OH electrooxidation activity compared to Pt only. They suggested that the difference between theirs and previous work lies in the better stability of the PtSn alloys in acidic solutions and suggested that the reported CH_3OH electrooxidation activities for nonalloyed Pt/Sn catalysts is due to the dissolution of Sn from the catalyst surface. The dissolved tin is believed to form a Sn(II)/Sn(IV) shuttle in solution that does assist in the CH_3OH oxidation reaction to CO_2. Another point of view has been presented by Mukerjee and McBreen, who carried out X-ray absorption spectroscopy (XAS) studies on nanosized carbon-supported PtSn alloys and nanosized Pt carbon-supported catalysts with underpotential deposited Sn (Pt/Sn_{upd}) present at the surface [98]. They reference literature data that reported better CH_3OH electrooxidation activities of Pt/Sn_{upd} catalysts than for PtSn alloys. They explain the results based on measured differences in the

Pt—Pt bond distances between PtSn alloys and the non-alloyed Pt/Sn_{upd} catalysts. The Pt—Pt bond distances were obtained from XAS measurements. In the case of PtSn alloy catalysts, Pt—Pt bond distances of 0.28 nm were obtained, while a distance of 0.277 nm, i.e., similar to that of pure Pt, was found for the Pt/Sn_{upd} catalyst. The XAS studies suggest that the underpotential deposited Sn does not disturb the Pt structurally or electronically. In both cases, i.e., for the Pt/Sn_{upd} and the PtSn alloy catalyst, it was found that the surface Sn was associated with oxygenated species at all potentials. It was concluded that the structural changes of alloying Pt with Sn result in some inhibition of the ability of Pt to adsorb CH_3OH and dissociate C—H bonds. It is noteworthy that alloying Pt with Ru has a much smaller effect on the Pt—Pt bond distance than alloying with Sn; values of 0.274–0.267 nm are found, depending on the ruthenium content. This is to be expect, as Ru is a significantly smaller atom than Sn.

2.3.4. Pd

The influence of the addition of palladium to platinum based catalysts has been examined in at least one study. Gokagac et al. [99] prepared nanosized Pt, Pd, and Pt–Pd catalysts supported on carbon black. TEM investigations suggested the particle size was strongly influenced by the palladium content. For palladium-rich catalysts, rather large particles on the order of 150 nm were found to be formed, while the particle size was much smaller (less than 5 nm) for platinum-rich catalysts. The CH_3OH oxidation activities for the Pt, Pd, and a wide composition range of the Pt-Pd carbon supported catalysts were estimated using slow sweep cyclic voltammetry and constant-time transients recorded at constant potentials. They reported a beneficial catalytic activity for catalysts of 33 and 43 atom% Pd composition for the CH_3OH oxidation as compared to carbon-supported Pt catalyst particles. Slow sweep cyclic voltamograms recorded at 5 $mV\,s^{-1}$ suggest a lower CH_3OH oxidation onset potential, of ca. 50 mV, for CH_3OH oxidation at the best composition of the palladium-containing catalyst.

2.3.5. Platinum Nanoparticles on IrO_2 Substrates

Chen et al. [100] prepared Pt nanoparticles on IrO_2 substrates. They reported that the IrO_2 substrate assisted in the dispersion of the Pt particles and found that Pt particles of ca. 100-nm diameter were formed. They found a lower overpotential for the CO_{ads} oxidation reaction than for polycrystalline Pt, while the CH_3OH oxidation reaction did not seem to be catalytically beneficially affected. The mechanism of the decrease in the overpotential for the CO_{ads} oxidation reaction for the Pt particles on IrO_2 was addressed. The lower overpotential for the CO_{ads} oxidation reaction may be simply related to the fact that the CO_{ads} oxidation reaction generally takes place at lower potentials for smaller platinum particles as compared to the bulk metal system.

2.3.6. Multicompositions and Nanorod Systems

In some cases, very complex catalyst compositions have been tested such as PtRuRhNi [101]. These particular catalysts were prepared by the reduction of sodium borohydride, yielding a fine powder of very high surface area. Higher activities for the CH_3OH oxidation reaction than for Pt/Ru catalysts were reported. However, the electrochemical CH_3OH oxidation currents were not normalized for the real electrochemical Pt surface area. Closer inspection of the experimental data suggest that the PtRuRhNi catalyst system shows no true catalytic advantage with regard to lowering the onset potential for the CH_3OH oxidation reaction.

Liu et al. [102] prepared multisegmented PtNi nanorods with identifiable Pt-Ni interfaces. Ni-Pt, Ni-Pt-Ni, Ni-Pt-Ni-Pt, and Ni-Pt-Ni-Pt-Ni nanorods were prepared by sequential electrodeposition of the metals into the pores of anodic aluminium oxide membranes. The rods were ca. 170 nm in diameter and 1.6 μm in length with 530 nm of total Pt segment lengths. Field emission scanning electron microscopy (FESEM) backscattered electron images allowed the Pt and Ni segments to be distinguished. The Pt segments are brighter because of the higher atomic number of Pt. XRD characterization of the PtNi nanorods suggests that Pt and Ni are polycrystalline with face-centered cubic structures. XPS measurements suggest Pt and Ni are present at the surface in the Pt(0), Pt(II), Pt(IV), Ni(0), and Ni(II) states. The multisegmented nanorods were tested for the CH_3OH oxidation reaction at room temperature in 0.1 M $HClO_4$ + 0.5 M CH_3OH solutions using cyclic voltammetry. The data suggest a lower CH_3OH onset oxidation and oxidation peak potential than generally observed for pure Pt electrodes (polycrystalline and powder Pt), approximately in the 0.15 V range. The authors ascribe the CH_3OH oxidation activity to a role of the pair site bifunctional mechanism. This mechanism may be questionable, as one would expect the number of pair sites (Pt next to Ni) versus Pt sites without a Ni neighbor to be low in such segmented nanorods that appear to consist of no more than four Pt-Ni interfaces and long Pt and Ni segments. Furthermore, the CH_3OH oxidation activity for Pt only nanorods is not reported in this study. A comparison between PtNi and Pt nanorods would be useful to evaluate the mechanism and judge the validity of the proposed catalytic effect of the Pt-Ni pair sites.

2.4. Oxidation of Solution CO

The electrooxidation of solution (gaseous) CO is an equally important topic as the electrooxidation of CH_3OH and adsorbed CO, as the use of H_2 contaminated with CO is of interest to fuel cell technology. The electrooxidation characteristics of CH_3OH, adsorbed CO and solution CO are generally different. Similar to the electrooxidation of CH_3OH, a bifunctional mechanism is proposed for the oxidation of solution CO and nanosized catalysts are important to optimize the catalyst surface area to bulk atom ratio. The catalyst particle size influence for the oxidation of solution CO has attracted little attention. However, there are a number of studies that discuss the preparation, electrooxidation activities, properties, and characterization of nanosized Pt-based catalysts that are typically supported on carbon black. Pt/Ru catalyst systems show a good activity for the dissolved CO electrooxidation reaction. Contrary to the CH_3OH electrooxidation reaction, catalysts other than Pt/Ru also show good electrocatalytic activities

for the oxidation of solution CO. These are Pt/Sn and Pt/Mo oxide [98, 103, 104]. For the Pt/Mo oxide catalyst systems, a series of studies has been carried out by Mukerjee and McBreen using *in-situ* XAS methods [104]. They reported a 3 times better CO tolerance of a carbon supported nanosized Pt-Mo catalyst over a state of the art carbon-supported Pt/Ru catalyst. It is noteworthy that no such enhancement was observed for the case of the CH_3OH electrooxidation reaction for the Pt/Mo oxide catalyst. The average Pt/Mo oxide particle size was 3–3.5 nm, as identified from TEM images. XRD studies showed a high degree of crystallinity and a fcc lattice for the platinum that appears to be typically observed for the fuel cell catalysts. The *in-situ* XAS studies suggest a redox couple on the Mo surface involving the V+ and VI+ states in the presence of both CO and CH_3OH. This is fundamentally different from Pt/Ru catalysts, for which the majority of the studies suggest the Ru to be present in the metallic, oxide-free form in the presence of CO and CH_3OH. XAS characterization of the nanosized Pt/Mo oxide catalysts suggests a negligible perturbation of the platinum lattice parameter in the presence of molybdenum. The majority of the Pt/Mo oxide catalysts were purchased from E-Tek, with the exception of the Pt to Mo 50:50 atom% composition that was prepared in-house. In theoretical work in which nanometer scale metallic clusters were studied, it was suggested that the Pt/Mo oxides have a strong tendency for chemical ordering. This finding was supported by experimental studies that suggested that Mo does not form pure clusters but does form bimetallic ones having the fcc structure. XAS studies indicate that Mo atoms are deposited epitaxially onto Pt clusters. In the presence of heteroatomic bonds, this Pt–Mo interaction helps to maintain the Pt in a highly dispersed form with supported Pt clusters smaller than 1 nm. Nanosized Pt/Sn catalysts have also been studied for the electrooxidation reaction of solution CO [97, 105–107]. Carbon-supported nanosized Pt/Sn catalysts have been prepared by using a wide variety of methods. These include impregnation and spontaneous deposition combined with dip coating of Sn [97, 105–108]. Different Pt/Sn catalysts were made such as PtSn alloys and tin preferentially deposited onto the Pt surface. To the best of our knowledge, a definitive comparison of the electrocatalytic activity for the oxidation of solution CO for alloyed versus nonalloyed Pt/Sn catalysts has not yet been made. Based on the XAS results reported by Mukerjee and McBreen for the case of the CH_3OH electrooxidation reaction and the fact that Sn undergoes underpotential deposition (upd) onto Pt surface, one would expect the nonalloyed Pt/Sn catalysts prepared by upd of Sn onto Pt to have a good CO electrooxidation activity [97]. Radmilovic et al. carried out a microstructural characterization of three commercially available carbon-supported Pt/Sn catalysts [107]. All three catalysts were prepared by conventional precipitation methods; however, different temperatures (500 vs. 900°C) were utilized to decompose the precursor salts in inert N_2 atmospheres. All catalyst particles were of 6 ± 3 nm average particle size as revealed by low-resolution TEM. At higher resolutions, differences in particle shape and composition became apparent. It was concluded that the three Pt/Sn catalysts have different coordinations. This is expected to result in different catalytic activities if these differences are relevant to the reaction.

A fundamental difference between the Pt/Ru and the Pt/Sn, as well as the Pt/Mo-oxide catalysts, is the state of the "admetal" under fuel cell operating conditions, i.e., also in the presence of CO and CH_3OH. Surface Sn and Mo are present as oxides at which CO does not adsorb, while surface Ru is present in the metallic form, thus allowing CO to also adsorb on Ru sites. The presence of surface oxides actually assists in the oxidation of dissolved CO, as the formation of OH is not hindered by adsorbed CO. This is in fact seen by lower oxidation potentials for solution CO than for the oxidation of a monolayer of adsorbed CO for the Pt/Sn and the Pt/Mo oxide catalysts, while the reverse trend is observed for Pt/Ru catalysts [108]. In both cases, i.e., for the Pt/Sn and Pt/Mo oxide catalysts, stability in an acidic environment is an issue, and care must be taken to work at sufficiently low anode potentials.

Schmidt et al. [109] reported a Pt-free bimetallic catalyst system having superior activities for the oxidation of CO. In their study, the CO was present at high concentrations in the H_2 fuel. They prepared Pd/Au nanoparticles of ca. 6 nm size on carbon black using the "Boennemann" method. They tested their catalysts for the oxidation of CO in H_2 and compared the performance to Pt/Ru carbon-supported nanosized catalysts. They reported an improved performance for H_2 anode fuels containing 1000 and 250 ppm CO for the Pd/Au nanosized catalysts at 60°C. They proposed that the observed improved CO tolerance mechanism at low overpotentials for the PdAu nanocatalyst electrodes is governed by a lower CO steady state surface coverage compared to the state of the art Pt/Ru carbon-supported catalyst electrodes. This was proposed to be due to a lower CO adsorption energy and finite CO oxidation rates on the Pd/Au catalyst, which both result in free surface sites for H_2 oxidation to take place. The reader should note that the effect is more pronounced at higher temperatures (60°C) and is observed for very high (1000 and 250 ppm) CO concentrations in the H_2 fuel.

2.5. Challenges for the Characterization of Nanosized Catalysts and Catalyst Surface Structures

Proper characterization tools are essential for the development of catalysts and to understand the catalyst structure–activity relationship. Typical methods available are high-vacuum methods that allow *ex-situ* characterization of the catalysts. Such methods are TEM, SEM, FESEM, Auger, and XPS. A number of methods are also available for *in-situ* characterization of the catalysts. One method is X-ray absorption fine structure (EXAFS), which is a powerful tool for the investigation of the local structure of metal cluster particles. The method can be used to study colloidal metal particles in dispersion and metal particles supported on substrates. EXAFS measurements provide information about the environment around a particular metal atom in the metal cluster such as the number and the kind of neighboring atoms as well as their distances from the X-ray absorbing atom, without the requirement for long-range order. EXAFS is an average technique, thus it needs to be complemented with techniques that yield information about single particles such as high-resolution transmission microscopy (HRTEM).

The characterization methods are often demanding and work intensive and require expensive instrumentation. However, they are often the only methods available to get reliable information regarding the catalyst particle size, agglomeration, and lattice parameters. X-ray diffraction (XRD) is a less work intensive method and suitable for initial screening of catalyst bulk properties. However, in the case of nanosized catalysts the intensity of the XRD pattern is low. The diffraction peaks broaden with a decrease in particle size, thus resulting in a decrease in the accuracy of the extracted data such as the lattice parameter from raw XRD results. Electrochemical methods such as the oxidation characteristics of adsorbed CO are also being tested to probe their suitability to characterize catalyst surface structures and catalysts in the nanosize range.

2.5.1. Potential Use of Organic Test Molecules as Surface Probes for Electrocatalysts

The use of test molecules to probe and characterize catalyst surface structures via electrochemical oxidation studies can be useful. This has been discussed (see above) for the case of the electrooxidation reaction of CO_{ads}. Another useful test method is the electrooxidation reaction of $(COOH)_2$. This has been tested for unsupported high surface area platinum and Pt/Ru catalysts [110]. Platinum is a catalyst for the electrooxidation of $(COOH)_2$. In fact, the overpotential for the electrooxidation of $(COOH)_2$ is roughly 80 mV lower for platinum than for gold, and no $(COOH)_2$ oxidation current is observed when ruthenium is used as electrode material. This catalytic advantage of platinum for the $(COOH)_2$ oxidation reaction can be used to obtain a measurement for the electroactive platinum surface area for pure platinum and multicomponent platinum systems via the measurement of the activation controlled $(COOH)_2$ oxidation current. Furthermore, the combination of the CO_{ads} oxidation charge and the electroactive surface area, obtained using the $(COOH)_2$ oxidation method, can be used to obtain information about the oxidation state and distribution of the admetal. The method has been applied to a range of high surface area Pt/Ru catalysts and useful information about the make-up of the catalyst surfaces were obtained. The principles of this method have also been applied to obtain true catalytic activities for a number of platinum-based catalyst systems [111].

Another simple *in-situ* method that allows for probing the oxidation state of the ruthenium adcomponent during an electrochemical oxidation reaction has been suggested more recently [112]. The method has also been applied to obtain *in-situ* information about unsupported platinum and Pt/Ru catalysts during the CH_3OH electrooxidation reaction. It involves the monitoring of the potential decay as a function of the time when a galvanostatic reduction current is applied after the electrooxidation reaction of the molecule of interest has been carried out. In light of the bimetallic reaction mechanism, the method suggested that ruthenium in its metallic form is the active form at which the formation of OH needed for the complete CH_3OH to CO_2 oxidation reaction takes place. The approach also yields information about the Pt to Ru surface site distribution.

2.5.2. X-ray Diffraction

X-ray diffraction spectroscopy (XRD) carried out in the reflection mode is often performed on carbon-supported nanosized Pt-based fuel cell catalysts. The small particle size results in very broad peaks and low intensities. Frequently, the peak width is used to calculate the particle size of nanosized catalyst systems. One, however, needs to remember that the peak width is influenced by a number of factors such as stress in the sample. It also yields an average number, and agglomeration of individual particles is not recognizable in the XRD pattern. XRD also gives information about possible alloying of the catalyst components, e.g., dissolution of Ru in the Pt lattice. The two theta peak position can be used to indicate alloying as well as the degree of alloying. However, in the case of powders, an internal standard needs to be used to correct for possible sample displacement effects. One also needs to remember that the accuracy of the peak position is affected by the broadness of the diffraction peak typically observed for nanosized particles. Factors such as stress and substrate influences (the latter becoming increasingly more relevant as the particle size decreases) affect the peak position as well. Alternatively, the transmission XRD mode can be used to study carbon-supported nanosized catalyst particles. Adora et al. [113] tested and compared the use of X-ray powder diffraction with synchrotron radiation in the standard and anomalous mode to study Pt particles deposited on carbon paper. They concluded that they could straightforwardly determine the mean diameter and the surface concentration of the carbon-supported Pt nanoparticles, even down to diameters of 2–3 nm and catalyst amounts of 0.03 $mg\,cm^{-2}$. The anomalous small-angle X-ray scattering (ASAXS) experiment, combined with synchrotron radiation, allows the catalyst scattering to be retrieved from the large porosity background. It is noteworthy that there is no mention of measuring and, hence, confirming the Pt particle size data obtained from the synchrotron studies by TEM in the work by that group. Such a measurement is useful in order to validate the XRD method. Higher sensitivity is achieved using the X-ray diffraction method when coupled with synchrotron radiation. This defines the peak position and shape better, and hence, any values calculated using these data are more accurate. However, the same limitations apply as for XRD in general; i.e., particle sizes calculated from peak half-widths reflect average values, etc.

2.5.3. In-Situ Electrochemical and Infrared Spectroscopy

Infrared spectroscopy (IR) carried out *in situ* with electrochemical experiments is a popular method to study the electrode/solution interface. Species formed and adsorbed on the electrode surface can be identified. The methods have also been applied to study nanosized catalyst systems [114–121]. Christensen et al. [114] extended the *in-situ* IR studies to carbon-supported Pt nanoparticle electrodes, showing that the particle size alters the onset of the CH_3OH chemisorption reaction. In the case of nanosized catalysts, the preparation of the electrode becomes a point of discussion. Typical *in-situ* electrochemical IR experiments have been carried out in the reflectance mode, where a smooth and IR reflecting electrode surface is needed. Typically fuel

cell catalysts are deposited on carbon black, i.e., onto a rough and IR nonreflecting surface. Friedrich et al. [115] deposited very small amounts of carbon-supported catalysts onto gold substrates and studied the adsorption of CO on the Pt nanosized particles. The amount of Pt on carbon deposited was sufficiently small, thus allowing the IR light to penetrate the carbon supported catalyst particles. Weaver et al. described a simple method for preparing metal nanoparticle films immobilized on gold substrates [116]. For these thin films, the anomalous bipolar and inverted IR band effects typically observed for thick and densely packed films were absent. In order to achieve a well-distributed metal nanoparticle array, the gold substrates were pretreated with 3-mercaptopropyltrimethoxysilane before anchoring gold, platinum, or platinum–ruthenium alloy nanoparticles onto the substrates. The prepared nanoparticle films displayed excellent electrochemical properties, implying facile electronic communication through the organic glue matrix between the nanoparticle arrays and the gold substrate. Coating of the gold nanoparticle arrays with platinum via copper underpotential deposition was also found to demonstrate optimal electronic response between the nanoparticle arrays and the underlying substrate. These findings are believed to facilitate the analysis of nanoparticles via *in-situ* electrochemical FTIR spectroscopy.

In another approach, Moon et al. set up and utilized attenuated reflectance spectroscopy (ATR) in combination with electrochemistry and showed that the method could be used to study thick layers of nanosized platinum catalysts supported on carbon black [117]. The method involved the setup of a thin electrolyte layer ATR-FTIR technique. Commercially available ATR crystals and a crystal-electrode setup in the Otto configuration were used. The technique also allows the detection of reaction products formed in solution as a result of the electrochemical reaction. The optically "thick" catalyst layer, however, results in bipolar (negative) bands. The occurrence of negative bands can be avoided if optically sufficient thin layers are used, as pointed out by Stamenkovic et al. [118], who studied the influence of the catalyst layer thickness onto adsorbed CO bands using *in-situ* infrared reflection-absorption spectroscopy (IRAS). They developed a so-called temperature-induced deposition method to deposit nanosized catalysts supported on carbon onto suitable substrates. Their idea is in many ways similar to the method used by Friedrich et al. [115]. Stamenkovis's et al.'s method to deposit the thin layer on the electronically conducting substrate is more refined and described in great detail. They use a hot plate to heat the substrate onto which the dispersed carbon supported catalysts are pipetted in small volumes and subsequently dried. The entire process is carried out under controlled, inert atmosphere.

A number of *in-situ* IR studies have involved the investigation of adsorbed CO and CH_3OH oxidation on bulk Pt and Pt nanoparticles [119–121]. The Stark tuning rate has been the object of a number of these studies involving the *in-situ* IR study of adsorbed CO on catalyst surfaces. The Stark tuning rate is the slope of the infrared vibrational stretch frequency to the electrode potential. Generally, the more positive the electrode potential, the higher the stretching frequency. Rice et al. [119] showed that the infrared stretch frequency and the Stark tuning rate strongly depend on the Pt particle size. Pt catalysts of 2, 2.5, 3.2, 3.9, and 8.8 nm average particle size were tested. Their study was coupled with ^{13}C electrochemical (EC) NMR studies. IR gives information about the bond strength of adsorbed CO, while ^{13}C EC NMR gives additional, more quantitative insight into the CO—metal bond. Based on the ^{13}C EC NMR studies, the observed dependence of the Stark tuning rate with the Pt particle size is due to the variation in the $2\Pi^*$ back-donation from metal to CO caused by strong interactions between Pt nanoparticles and the conductive support. A decrease in the vibrational frequency for adsorbed CO with particle size smaller than 4 nm was observed, while the frequency was essentially independent of the particles size larger than 4 nm.

Weaver's research group used *in-situ* IR to study the oxidation rates of HCOOH, formaldehyde, and CH_3OH for different Pt particles sizes [120]. Carbon-supported Pt particles in the size range of 2–9 nm were used in his study. Particle size influences on the oxidation rates per Pt surface were observed for particles of less than 4 nm diameter, while the rates for larger particles were essentially the same as for bulk metal Pt electrodes. In case of CH_3OH, a decrease in the oxidation rate with particles size was observed, while the HCOOH oxidation rate increased with decreasing Pt particle size. Essentially no dependence on the Pt particle size was found for the oxidation rate of formaldehyde. They explained the observed differences in the rates due to differences in the availability of Pt terrace sites, i.e., using a similar argument as Kinoshita for the case of the O_2 reduction reaction. In the case of the CH_3OH oxidation reactions, the Pt terrace assembly that favors dehydrogenation and CO adsorption are proposed to decrease with decreasing particle size.

In a very recent paper, Arenz et al. used *in-situ* IR to study the behavior of adsorbed CO on Pt particles of sizes varying between 1 and 30 nm [121]. The study was combined with TEM characterization of the carbon-supported Pt particles. The TEM images showed the bigger Pt particles to have a larger surface than the small particles, which showed fairly smooth Pt(111) facets. The Pt catalysts used in the study were commercially available. The smaller Pt particles were supported on high surface area carbon, while the larger particles were supported on the 3M whiskers (see Section 2.1.2, this chapter). It was proposed that the defects play a significant role in the resulting CO "clustering" on the nanoparticles. Furthermore, the CO ad-layer oxidation is proposed to be predominantly influenced by the ability of the surface to dissociate water (−OH formation) at defect sites rather than by the CO energetics on the catalyst surface.

(a) CO and IR as Surface Probe for Nanocatalyst Particle Structure. Vibrational spectra of adsorbed CO is frequently used to probe the surface structure of nanosized catalysts [122–129]. Many of these studies have been carried out in solutions where the catalysts are present as colloids. Note that these studies do not involve electrochemical measurements. They are pure spectroscopic measurements. Studies have been reported for hydrosols of platinum, palladium, and rhodium and organosols of nickel, palladium, platinum, ruthenium, and palladium–copper alloys [122–127]. In two recent reports, de Caro et al. [128, 129] studied the vibrational spectra of adsorbed CO for Pt colloids stabilized

using poly(vinylpyrrolidone). They focused their study on IR absorption frequencies of adsorbed ^{12}CO and mixtures of ^{12}CO–^{13}CO. Phenomena such as coverage-dependent frequency shifts and nonlinear intensity ratios for ^{12}CO–^{13}CO mixtures were applied to the Pt nanocatalysts, as they can be used to provide information about the structure of the catalyst surface. Colloidal particles typically have irregular surfaces, i.e., defect sites, thus resulting in the abundance of CO domains. The study of the vibrational CO adsorption spectra of colloidal catalyst solutions offers the advantage that fast adsorption equilibria are reached during the addition of the adsorbate, as compared to supported solid catalysts, where mass transport limitations of the adsorbate into the porous and high surface area structure are typically observed. However, the presence of the stabilizing agent could interfere with the CO adsorption assembly. The latter needs to be considered for the study of the vibrational adsorption spectra of nanosized catalysts supported on electronically conductive substrates as well. Park et al. [130] carried out an extensive IR study of the adsorbed CO on carbon-supported Pt catalysts. They used a wide range of Pt particle sizes below and above 4 nm average particle size. The IR spectra were compared with spectra for single-crystal electrodes and high-nuclearity carbonyl clusters. The IR spectra for the adsorbed CO are clearly dependent on the Pt particles for smaller sized particles (ca. 2–4 nm) and differences in the adsorption frequency as well as peak width of the vibrational CO adsorption peak. A red shift in the frequency was observed as the particle size decreased. Frequency changes on the order of 40 cm^{-1} were reported. The Stark tuning rate was found to be independent of the particle size. Furthermore, the smaller particles were observed to exhibit a lower wavenumber "tail," although the overall bandwidth narrows with decreasing particle size. In a number of studies [131–133] involving high-index monocrystalline Pt surfaces, it has been established that CO bound to step or edge sites exhibit CO frequency values 20–30 cm^{-1} lower than for terrace bound CO, and the sharp decrease in the frequency of the adsorbed CO for particles of less than 4 nm diameter was assigned by Park et al. to a transition from predominantly (111) terrace to edge site CO binding for the smaller carbon-supported Pt particles. The results were also compared to theoretical density functional theory (DFT) studies of CO chemisorbed on steps, kinks, and terraces [134]. The study suggested that an increase in the d-band energy, i.e., an increase in the local Fermi-level density of states, is associated with a stronger binding energy of CO on step and kink sites of platinum. It should be noted that Friedrich et al. [115] also reported changes in the frequency of adsorbed CO on Pt colloids deposited onto gold substrates. They observed shifts in the frequency to higher values as the coverage of the Pt particles increased. The shift was determined to be introduced by particle agglomeration and larger particles at higher Pt loadings.

2.5.4. NMR Characterization of Nanoparticles and Electrooxidation Reaction on Nanosized Catalyst Surfaces

NMR spectroscopy can also yield very valuable information about nanoparticles and species adsorbed on nanosized catalysts. The first report to use NMR spectroscopy for the direct detection and characterization of platinum nanoparticles is by Fraissard [135]. Platinum is well-suited for NMR studies, as it can be detected by NMR spectroscopy. Therefore, the shape of the NMR spectra can be related to the dispersion of the metal, and the electron density of states at the Fermi level can be calculated. This analysis of NMR spectra was first applied to platinum, palladium, and rhodium nanoparticles. The ^{195}Pt nucleus has a sufficient natural isotopic abundance (33.7%), a reasonably high gyromagnetic ratio to the frequency, and a spin of 1/2, which eliminates the complexity of structure on the NMR line shape that arises from electric quadruple moments. In metals, the conduction-electron spins are polarized by the magnetic field, giving raise to an additional shift in the frequency. This is called the Knight shift. Platinum has a large negative Knight shift, which makes it possible to resolve the shifts of atoms in the surface layer versus the bulk atoms. The chemical shifts of surface atoms is also influenced by adsorbed molecules and in fact depends on their nature. Wieckowski's research group has made extensive use of these facts and used NMR spectroscopy to characterize nanosized Pt and Pt/Ru catalysts [136, 137]. Based on the ^{195}Pt NMR studies for high surface area platinum black and PtRu alloys of apparently similar particle size, a surface enrichment of platinum atoms in the PtRu alloy catalyst was found [137]. Furthermore, the ^{13}C NMR spectra for CO adsorbed on the PtRu alloy was observed to consist of a single peak, exhibiting only a small Knight shift. ^{13}C spin lattice relaxation results suggest that the addition of ruthenium causes a reduction in the Fermi level local density of states of the catalyst surface sites. This NMR result suggests electronic alteration of the catalyst surface sites by ruthenium. Electronic alterations, also referred to as ligand effects, of ruthenium in PtRu alloys have been suggested to also have a beneficial catalytic effect for the CO and CH_3OH oxidation reactions.

3. ROLE OF NANOSTRUCTURED ELECTRODES FOR ELECTROCHEMICAL ENVIRONMENTAL TREATMENT

The use of electrochemical methods for environmental treatments has attracted some attention [138–148]. The type of treatments involve anodic oxidation and direct oxidation reactions as well as reduction reactions of organic pollutants to valuable chemical products. The substrate plays a major role in all of these reactions. In the case of the oxidation reactions, the development of electrode materials that are very efficient, low cost, and stable for long periods of time under operating conditions is a crucial factor for the successful implementation of these technologies. The operating conditions, particularly in the case of the anodic oxidation reactions, are very harsh. Typically, very high current densities, i.e., positive potentials (larger than 1.2 V vs. the reversible hydrogen electrode (RHE)), are employed, thus limiting the number of electrode materials that are stable. Furthermore, O_2 is evolved in this potential range, which results in a decrease of the current efficiency. The mechanism of anodic oxidation has been discussed in a number of papers. There is a general trend to divide the reaction

pathway and resulting products into two groups depending on the "class" of electrode material [145]. The micro- and nanostructure influence on the oxidation reaction mechanism and efficiency of the process has attracted a very limited amount of attention so far.

Contrary to the case of the anodic oxidation reactions, the influence of the structure of cathodes has been studied widely and has been shown to play a crucial role in the outcome and product distribution of reduction reactions of organic "toxins" to potentially valuable organic chemicals [166–175]. Significant differences are observed between high surface area Raney-metal type electrodes versus the bulk metal analog [176–178]. As with everything, the use of electrochemical methods for wastewater treatment has advantages and disadvantages. One advantage of electrochemistry over, e.g., chemical and biological treatment, is its power to generate an "oxidant" or "reductant" *in-situ*, locally, and at high concentrations. The "oxidant" and "reductant" are typically used up in the reaction, and hence, separation between the treated water and process chemicals is not needed. The electrochemical reactions are heterogeneous, i.e., take place at the electrode surface, which, in turn, implies higher system costs. In particular, the initial capitol cost for an electrochemical reactor is larger than for a chemical or biological process that takes place in a homogenous phase. The cost of electricity can be high, for example, in Japan, while in other countries such as Canada electrochemical treatments are more cost attractive. The larger and more complex the toxin molecule, the more electrons are needed. For example, the complete oxidation of one phenol molecule to CO_2 requires 28 electrons, while the oxidation of $(COOH)_2$ requires only four electrons, thus the economics of the system is largely depend on the nature of the wastewater stream. Due to the nature of this chapter, focus is placed on the structure of the electrode catalysts. The interested reader can find detailed reviews about system designs, etc., elsewhere.

3.1. Anodic Oxidation Reactions

3.1.1. General Mechanism

For some time, the so-called anodic oxidation reaction, which is commonly also referred to as indirect electrochemical oxidation reaction, has been considered to be of technical relevance for the electrochemical treatment of wastewater. In 1991, Koetz and Stucki, from ABB in Switzerland, reported the oxidation of various organics using antimony "doped" tin dioxide electrodes [140, 141]. (Note that these electrodes are referred to as doped with antimony, even though the antimony content with roughly 4 wt% is rather high.) Their introduction of the antimony "doped" tin dioxide electrodes was considered to be a major improvement to the previously tested platinum electrodes [142]. The latter are (a) expensive and (b) prone to electrode fouling due to an organic film formation coupled with a decrease in activity. Comninellis research group, at the ETH in Lausanne in Switzerland, extensively investigated the anodic oxidation reaction [143–149]. Based on radical spin trap studies, they proposed the principles of the anodic oxidation reactions to rely on a preferably high concentration of hydroxyl radicals formed on the electrode surface [138, 146]. The hydroxyl radicals are proposed to be the key oxidant for the organic toxins to CO_2. It is suggested that they are preferably formed at electrode materials that exhibit high overpotentials for the oxygen evolution reaction (oer), while at low oer overpotential electrode materials, this species is not formed, hence, the division into "classes" of electrode materials (see above). Electrodes showing a high overpotential for the oer are antimony-"doped" tin dioxide, lead dioxide, and boron-doped diamond electrodes, while the noble metal oxide electrodes based on platinum, iridium, and ruthenium exhibit lower oer overpotentials. A very general reaction scheme for the oxidation of organic reactants (R) on metal oxide electrode surfaces (MO_x) has been proposed by the Comninellis group as summarized below [143, 145].

(a) Involvement of hydroxyl radicals:

$$MO_x + H_2O \rightarrow MO_x(^{\bullet}OH) + H^+ + e^-$$

$$MO_x(^{\bullet}OH) + R = MO_x + CO_2 + ze^- + zH^+$$

(b) Low oer overpotential electrodes, i.e., incomplete oxidation of the organic reactant is proposed:

$$MO_x + H_2O = MO_{x+1} + 2H^+ + 2e^-$$

$$MO_{x+1} + R = MO_x + RO$$

It should be noted that the formation of hydroxy radicals on the high oer overpotential electrodes has been proposed based on spin trap experiments. The spin trap is an organic compound, *N*,*N*-dimethyl-*p*-nitrosoaniline, and the rate of its partial oxidation is taken as a measurement of the hydroxyl radical concentration. It has not been investigated whether the spin trap molecule is actually directly oxidized on the electrode surface, i.e., without the need of hydroxyl radicals. Furthermore, in more recent work, it has been pointed out that for the full understanding of the oxidation mechanism, the nature of the organic compound needs to be considered. It has been shown that adsorption of organics on the electrode surface can play a major role in the oxidation mechanism. In the case of the oxidation of carboxylic acids such as HCOOH and $(COOH)_2$, adsorption is a prerequisite for their oxidation to CO_2. Bock et al. have prepared tungsten bronze oxide electrodes that contained Pt centers [149, 150]. In prior work, the platinum was proposed to be dispersed as microcenters within the electronically conductive tungsten bronze matrix [92, 151]. A detailed oxidation study carried out under potential control indicated that both of the two carboxylic acids, HCOOH and $(COOH)_2$, adsorb on the Pt centers and are oxidized to CO_2. The tungsten bronze is believed to mainly serve as electronically conductive backbone and substrate for the platinum centers. Depending on the experimental conditions, higher current efficiencies than for antimony-"doped" tin dioxide electrodes were achieved. The latter are considered highly active for the complete oxidation of these organics to CO_2. In the oxidation of $(COOH)_2$, the oxidation rate was found to be independent of the potential. This behavior suggests a reaction mechanism where the chemical reaction, namely, the breaking of the carbon—carbon bond of the $(COOH)_2$ molecule, is rate determining and the coverage of adsorbed $(COOH)_2$ on the electrode surface is high. It is likely that the cost of these electrodes based on

tungsten bronze containing platinum centers can be lowered through a higher dispersion, e.g., the use of nanosized platinum centers. Furthermore, the fact that the reaction rate of $(COOH)_2$ is independent of the potential suggests that such oxidation processes are preferably carried out at lower current densities and potentials. This has two beneficial influences, which are lower power requirements for the oxidation reaction and a higher efficiency of the process as less current is used to generate undesirable O_2.

The reaction mechanism shown above highlights the importance of the nature of the organic as well as the interplay between the organic and the electrode surface. For example, aromatic compounds like phenol can adsorb on electrode surfaces with different orientations, horizontal or perpendicular. The orientation depends on the phenol concentration and influences the product distribution. It has been shown for platinum electrodes that phenol-type compounds preferably adsorb horizontally at low concentrations, while at higher concentrations the molecules preferably adsorb perpendicular [152].

3.1.2. Electrode Structure Influence

Very little emphasis has been placed in the study and optimization of the electrode structure on the efficiency of the oxidation reaction process of organics. On the contrary, the majority of the studies focused on the electrode material, and, indeed, electrode materials that also showed large differences in electrode structure and level of porosity, in addition to their chemical composition, were often compared. The importance of the porosity of the electrode material has been shown in one study [153]. In this study it was shown that the oxidation rate for low oer overpotential electrodes can be as high as for high oer overpotential electrodes. In fact, oxidation rates of IrO_2 based dimensionally stable (DSA) electrodes were estimated to be as high as for antimony-doped tin oxide electrodes. The IrO_2 electrodes were diluted with different amounts of TiO_2 and CeO_2, and IrO_2 only electrodes were prepared at different temperatures. Electrodes with different IrO_2 surface areas were achieved in this manner. In case of the IrO_2/TiO_2 and the $IrO_2/TiO_2/CeO_2$ DSA type electrodes, the IrO_2 sites are active for the oer, i.e., these electrodes are classified as low overpotential electrodes for the oer. The oxidation rate of *p*-benzoquinone was studied under rapid stirring conditions, i.e., ensuring that the reaction was not limited by mass transport limitations. The reaction was found to be faster with an increase in current density, i.e., also an increase in electrode potential, thus further indicating that the reaction is not controlled by mass transport limitations. A direct correlation between the IrO_2 surface and the reaction rate of *p*-benzoquinone was observed. This suggests that anodic oxidation studies need to consider the electrode structure and nature, as well as the nature of the organic test molecule. The oxidation reactions were carried out under constant current application, as is frequently done for these studies. However, one should note that proper reaction mechanism studies need to be carried out under potential control. While, current control is more relevant for practical application, depending on the nature of the reaction, e.g., activation versus mass transport controlled, the electrode potential can shift drastically, thus making the interpretation of data in regards to thermodynamical processes very complex or most likely impossible.

It appears logical that the cost of electrodes based on expensive noble metals could be reduced by fabricating electrodes that consist of nano- or micrometer-sized catalyst centers within a stable, electronically conductive, and inexpensive electrode matrix. This approach has been investigated in one study [154]. Comninellis's group deposited different loadings of IrO_2 and RuO_2 nanoparticles on boron-doped diamond substrate and tested the electrodes for various oxidation reactions. As expected, with an increase in IrO_2 and RuO_2 loading, a decrease in the overpotential for the organic oxidation reaction such as hydroquinone and the Cl_2 evolution reaction was observed. For very high loadings of the noble metal oxides, the oxidation characteristics of these reactions were observed to approach the well-known behavior for their DSA equivalent, i.e., bulk IrO_2 and RuO_2 electrodes. The work shows that boron-doped diamond can be used as a stable substrate for nanosized electrocatalysts. Lower loadings of the expensive noble metal oxides are possible on boron-doped diamond electrodes than the commonly used titanium substrates. Unfortunately, the price of boron-doped diamond electrodes is high.

3.2. Electrochemical Promotion of Catalysis

A relatively newly discovered phenomena is the electrochemical promotion of catalysis (EPOC) [155–159]. For this process, very thin films of, e.g., IrO_2 or Rh, are deposited onto Y_2O_3 stabilized ZrO_2 (YSZ) and on YSZ coated with a thin porous layer of TiO_2 (TiO_2/YSZ) and serve as the working electrodes. The oxide, i.e, YSZ, serves as O^{2-} conductor and separator between cathode to anode. Catalytic rates for nonfaradaic processes such as the preferably selective oxidation of CH_4 to CO and H_2 can be enhanced upon the application of a small current to these systems. This reaction, the production of syngas from CH_4, is of great industrial interest, and the catalytic partial oxidation route to generate syngas is more energy efficient than the traditional steam reforming process. In the case of the Rh films, the electrochemical enhancement is reversible, while in the case of IrO_2, it is irreversible; i.e., in the latter case the catalytic advantage remains after the electrochemical treatment. Increases in catalytic rate of up to 5 orders in magnitude more than anticipated for the rate of supply or removal of O^{2-} to the catalyst electrodes have been observed for the EPOC. In very recent work, it has been shown that the EPOC process can be effectively applied to thin (40 nm) Rh films on YSZ and TiO_2/YSZ electrodes [157–159]. The thin film Rh electrodes were used to study the oxidation of ethylene to CO_2, as a model reaction as well as for the selective oxidation of methane to syngas. The work showed the concept of using electrodes made of films of noble metals in the nanothickness level to successfully produce syngas and as EPOC catalysts.

3.3. Electrochemical Reduction of Nitrates

The reduction of nitrate and nitrite is of high environmental interest. Nitrate and nitrite are very widespread and

problematic contaminants in ground and surface waters, particular in areas of high agricultural activities. Chemical reduction, biological treatments, reverse osmosis, and ion exchange are being examined; however, electrochemical reduction treatments of nitrate and nitrite are being considered as possible alternative routes [160–165]. The electrode (cathode) material plays a significant role in the NO_3^- reduction reaction to, preferably, N_2. The general reduction scheme and possible reaction pathways are as follows [161]:

$$NO^-_{3(aq)} \leftrightarrow NO^-_{3(ads)} \rightarrow NO^-_{2(ads)} \rightarrow NO_{(ads)} \rightarrow NO_{(aq)}$$

$$NO^-_{2(ads)} \rightarrow NO^-_{2(aq)}$$

$$NO_{(ads)} \rightarrow N_2O \rightarrow N_2$$

$$NO_{(ads)} \rightarrow N_2$$

$$NO_{(ads)} \rightarrow NH_3$$

The reduction reaction is complicated and the selectivity and rate of reduction is influenced by a number of factors such as the cathode material and solution pH. De Voovs et al. [161] prepared copper electrodes on palladium substrates by underpotential deposition (upd) of copper. Using upd, the electrode surface structure could be controlled in the submonolayer range. It was concluded that the copper is needed to facilitate the first electron transfer reaction, i.e., $NO^-_{3(ads)} + e^- = NO^-_{2(ads)}$, while the palladium steers the subsequent reaction selectivity toward the production of N_2. A number of cathode materials other than the Cu/Pd system have been tested for the NO_3^- reduction reaction such as platinum and palladium substrates modified with sublayers of tin. The latter are proposed to have the highest activity for the reduction of nitrate. The cathode structure appears to have a very strong influence on the reduction reaction of nitrate. In a very recent publication, Tucker et al. [165] explored a process to roughen thin films of rhodium that have been deposited on titanium substrates. The process was referred to as activation of the rhodium electrode for the nitrate reduction reaction. The surface roughening was induced by dissolving rhodium by potential cycling in alkaline solutions also containing chloride and nitrate. Based on subsequent cyclic voltammetry studies of the electrode surface, it was concluded that the hydrogen upd and the $-OH$ adsorption reaction behave differently, thus indicating morphological changes of the electrode surface. So-called nanostructured "sponge" electrodes of high surface area (roughly 19 $m^2\,g^{-1}$) and particle sizes in the 7–10 nm range were formed in this manner. Product analysis does not seem to have been carried out in this very recent study.

3.4. Role of Electrode Materials for Electrochemical Hydrogenation Reactions

The hydrogenation of organic compounds is an important class of reactions and has been extensively studied in gas and liquid phase [166]. Liquid phase hydrogenation can be carried out catalytically, typically at high pressures and temperatures, while the reactions can also be carried out electrocatalytically. The electrocatalytic hydrogenation (ECH) reaction has the advantage of milder reaction conditions [167]. In the latter area, advances have been made through the development of new electrode materials, namely, massive electrodes, powder cathodes, and polymer film electrodes in combination with the determination of the best reaction conditions. The general reaction scheme for the ECH is described as follows for an electrode material (M) and an organic R-X:

$$2H_2O + 2e^- + M \rightarrow 2(H)_{ads}M + 2OH$$

$$R\text{-}X + M \leftrightarrow (R\text{-}X)_{ads}M$$

$$(R\text{-}X)_{ads}M + 2(H)_{ads}M \rightarrow (R\text{-}H)_{ads}M + HX$$

$$(R\text{-}H)_{ads}M \leftrightarrow R\text{-}H + M$$

The competing reaction (if hydrogenation reaction is too slow with respect to H_2 evolution reaction), is the following:

$$(H)_{ads}M + H_2O + M + e^- \rightarrow H_2 + 2OH^-$$

$$(H)_{ads}M + (H)_{ads}M \leftrightarrow H_2$$

ECH has several advantages over catalytic hydrogenation. As seen in the equations above, H_2O is the source of the hydrogen present in MH_{ads}. Hence, ECH has two advantages, as the kinetic barrier due to the splitting of H_2 is circumvented and the mass transport of the poorly soluble hydrogen molecules is not an issue. Elevated temperatures and high pressures can be avoided in the ECH, thus presenting milder reaction conditions. Furthermore, electrochemistry provides the means to control the amount of chemisorbed hydrogen through the control of the current density or potential.

The nature of the electrode material and the nature of the electrode surface (which depends on the history of electrode preparation) are major factors influencing the efficiency and product distribution of the ECH process. Many studies have been carried out using noble metal catalysts, as they are catalytically very active. Platinum, palladium, and rhodium are of particular interest [168–170]. Effort has been placed on dispersing the metal particles in conducting polymers or using carbon-supported catalyst systems [171–173]. The incorporation of metallic particles into conducting porous polymer matrixes for ECH reactions also provides the advantage of minimizing particle agglomeration and reduces the risk of loss of the particles, thus increasing the lifetime of the catalysts. Dispersed metal catalysts studied were platinum, palladium, rhodium, and ruthenium. Other electrode materials consist of Raney type (Raney nickel, Raney cobalt, and Raney copper) and spongy transition metal electrodes [174, 175]. The powdery nature of these high surface area electrodes complicates the extraction of the hydrogenated products and the recovery of the catalyst, as compared to solid electrodes. Lessard's research group prepared more convenient Raney nickel type electrodes that also show longer lifetimes than the conventional Raney nickel type electrodes [176, 177]. Their electrodes consisted of Raney nickel particles embedded in a nickel matrix. The electrodes were prepared in a series of subsequent steps, as follows: Particles of the Raney alloy, suspended in a nickel bath, were electroplated onto a stainless steel grid. Subsequently, the high surface area electrode structure was obtained by leaching the aluminum in the alloy in a sodium

hydroxide solution, i.e., using a standard procedure to prepare Raney nickel. In many studies, the importance of using high surface area electrodes, as compared to the bulk metal analog, is shown [171, 176, 178, 179]. For example, the use of Devarda copper electrodes showed that nitrobenzene and nitrocyclohexane were electrohydrogenated to aniline and cyclohexylamine, respectively. The reactions took place with high efficiencies, while on a copper electrode only traces of aniline were found next to large amounts of the starting material and the undesired reaction product of azobenzene. Similar influences were found in the same study comparing the electrohydrogenation reactions of benzophenone, *N*-methyl-*p*-anisaldehyde imine using Raney nickel versus nickel plated electrodes.

Electrochemical hydrogenation reaction (ECH) is a very good method to selectively convert aliphatic nitro compounds to the corresponding aliphatic amines. ECHs offer high chemoselectivity and are, therefore, of real interest for the preparation of fine chemicals. Further improvements of the selectivity and efficiency of the process is required, which could make the ECH reactions sufficiently attractive to be used on an industrial scale.

4. FINAL WORDS FROM THE AUTHORS

It has been a pleasure to write this chapter, which is meant to include a comprehensive and updated review on electrochemical nanotechnologies applicable to environmental and energy conversion processes. Electrochemistry has played and is playing a major role in many relevant areas of interdisciplinary research and is of industrial importance in multiple areas in our society. The word interdisciplinary is of particular importance, and by undertaking a comprehensive review, one understands that electrochemistry is truly an assembly of multiple disciplines such as organic and organometallic chemistry, spectroscopy of all sorts, instrumental chemistry, physics, and material science, just to name a few. The importance of careful consideration and planning of research, working together as "teams" (where possible and beneficial), taking time to review and understand the work and thoughts of others is obviously essential for the success of this discipline. With such an organized, open, and thoughtful approach to both the fundamentals and applications of electrochemical science and technology, it is possible to put in place the building stones for integrated and successful research and development in this area.

ACKNOWLEDGEMENTS

We thank Prof. E. Gileadi (Tel-Aviv, University) and Dr. Y. LePage (National Research council of Canada) for very helpful discussions.

REFERENCES

1. J. O'M. Bockris and H. Wroblowa, *J. Electroanal. Chem.* 7, 428 (1964).
2. M. Watanabe and S. Motoo, *J. Electroanal. Chem.* 60, 267 (1975).
3. H. A. Gasteiger, N. Markovic, P. N. Ross, and E. J. Cairns, *J. Electrochem. Soc.* 147, 1795 (1994).
4. B. Gurau, R. Viswanathan, R. Liu, T. J. Lafrenz, K. L. Ley, E. S. Smotkin, E. Reddington, A. Sapienza, B. C. Chan, T. E. Mallouk, and S. Sarangapani, *J. Phys. Chem. B* 102, 9997 (1998).
5. T. Iwasita, H. Hoster, A. John-Anacker, W.F. Lin, and W. Vielstich, *Langmuir* 16, 522 (2000).
6. C. Bock, B. MacDougall, and Y. LePage, *J. Electrochem. Soc.* 151, A1269 (2004).
7. H. G. Petrow and A. J. Allen, United States Patent 4,044,193 (1977) .
8. F. G. Will, *J. Electrochem. Soc.* 110, 145 (1963).
9. V. G. Levich, *Acta Physicochim. URSS* 17, 257 (1942).
10. M. Eikerling, Y. I. Kharkats, A. A. Kornvshev, and Y. M. Volfkovich, *J. Electrochem. Soc.* 145, 2684 (1998).
11. E. Peled, A. Blum, A. Ahron, M. Philosoph, and Y. Lavi, *Electrochem. Solid State Lett.* 6, 12 (A268).
12. Q. P. Wang, M. Eikerling, D. T. Song, X. S. Liu, T. Navessin, Z. Xie, and S. Holdcroft, *J. Electrochem. Soc.* 151, A950 (2004).
13. Z. Xie, T. Navessin, K. Shi, R. Chow, Q. P. Wang, D. T. Song, B. Andreaus, M. Eikerling, Z. S. Liu, and S. Holdcroft, *J. Electrochem. Soc.* 152, A1171 (2005).
14. M. Uichida, Y. Aoyama, E. Eda, and A. Ohta, *J. Electrochem. Soc.* 142, 463 (1995).
15. M. Uichida, Y. Aoyama, E. Eda, and A. Ohta, *J. Electrochem. Soc.* 142, 4143 (1995).
16. M. Debe, in "Fuel Cell Technology and Applications" (W. Vielstich, A. Lamm, and H. Gasteiger, Eds.), Vol. 3, Part. 1, p. 576. John Wiley and Sons, 2003.
17. F. T. A. Vork, L. J. J. Janssen, and E. Barendrecht, *Electrochim. Acta* 31, 1569 (1986).
18. S. Holdcroft and B. L. Funt, *J. Electroanal. Chem.* 240, 89 (1988).
19. C. S. C. Bose and K. Rajeshwar, *J. Electroanal. Chem.* 333, 235 (1992).
20. H. Laborde, J. M. Leger, and C. Lamy, *J. Appl. Electrochem.* 24, 219 (1994).
21. J. Shan and P. Pickup, *Electrochim. Acta* 43, 2447 (1998).
22. T. Frelink, W. Visscher, and J. A. R. van Veen, *J. Electroanal. Chem.* 382, 65 (1995).
23. Y. Takasu, T. Iwazaki, W. Sugimoto, and Y. Murakame, *Electrochem. Commun.* 2, 671 (2000).
24. L. J. Bergoli, *Electrochim. Acta* 23, 489 (1978).
25. M. L. Sattler and P. N. Ross, *Ultramicroscopy* 20, 21 (1986).
26. M. Watanabe, H. Sei, and P. Stonehart, *J. Electroanal. Chem.* 261, 375 (1989).
27. K. Kinoshita, *J. Electrochem. Soc.* 137, 845 (1990).
28. S. Mukerjee and J. McBreen, *J. Electroanal. Chem.* 448, 163 (1998).
29. A. Rodriguez, C. Amiens, B. Chaudret, M. J. Casanove, P. Lecante, and J. S. Bradley, *Chem. Mater.* 8, 1978 (1996).
30. B. A. Sexton and G. E. Mitchell, *Surf. Sci.* 99, 539 (1980).
31. M. Watanabe, H. Igarashi, and T. Fujino, *Electrochemistry* 67, 1194 (1999).
32. T. Toda, H. Igarashi, H. Uchida, and M. Watanabe, *J. Electrochem. Soc.* 146, 3750 (1999).
33. T. J. Schmidt, U. A. Paulus, H. A. Gasteiger, and R. J. Behm, *J. Electroanal. Chem.* 508, 41 (2001).
34. U. A. Paulus, A. Wokaun, G. G. Scherer, T. J. Schmidt, V. Stamenkovic, N. M. Markovic, and P. N. Ross, *Electrochim. Acta* 47, 3787 (2002).
35. H. A. Gasteiger, S. S. Kocha, B. Sompalli, and F. T. Wagner, *Appl. Catal B: Env.* 56, 9 (2005).
36. F. Maillard, M. Eikerling, O. V. Cherstiouk, S. Schreier, E. Savinova, and U. Stimming, *Faraday Discuss.* 125, 357 (2004).
37. J. Meier, K. A. Friedrich, and U. Stimming, *Faraday Discuss.* 121, 365 (2002).
38. M. Del-Popolo, E. Leiva, H. Kleine, J. Meier, U. Stimming, M. Mariscal, and W. Schmickler, *Appl. Phys. Lett.* 81, 2635 (2002).

39. D. Hofmann, W. Schindler, and J. Kirschner, *Appl. Phys. Lett.* 73, 3279 (1998).
40. E. Budevski, G. Staikov, and W. J. Lorenz, "Electrochemical Phase Formation and Growth: An Introduction to the Initial Stages of Metal Deposition." VCH mbH, Weinheim, Germany, 1996.
41. E. Budevski and V. Bostanov, *Electrochim. Acta* 9, 477 (1964).
42. E. Budevski, V. Bostanov, T. Vitanov, Z. Stoynov, A. Kotzeva, and R. Kaischew, *Electrochim. Acta* 11, 1697 (1966).
43. E. Budevski, V. Bostanov, T. Vitanov, Z. Stoynov, A. Kotzeva, and R. Kaischew, *Phys. Status Solidi* 13, 577 (1966).
44. R. Kaischew and E. Budevski, *Contemp. Phys.* 8, 489 (1967).
45. J. V. Zoval, J. Lee, S. Gorer, and R. M. Penner, *J. Phys. Chem. B* 102, 1166 (1998).
46. H. Liu, F. Favier, K. Ng, M. P. Zach, and R. M. Penner, *Electrochim. Acta* 47, 671 (2001).
47. J. V. Zoval, J. Lee, S. Gorer, and R. M. Penner, *J. Phys. Chem. B* 102, 1166 (1998).
48. D. Richard and P. Gallezot, *Stud. Surf. Sci. Catal.* 31, 71 (1987).
49. H. A. Benesi, R. M. Curtis, and H. P. Studer, *J. Catal.* 10, 328 (1968).
50. T. J. Schmidt, M. Noeske, H. A. Gasteiger, R. J. Behm, P. Britz, W. Brijoux, and H. Boennemann, *Langmuir* 13, 2591 (1997).
51. L. Dubeau, C. Coutanceau, E. Garnier, J. M. Leger, and C. Lamy, *J. Appl. Electrochem.* 33, 419 (2003).
52. H. Boennemann, P. Britz, and W. Vogel, *Langmuir* 14, 6654 (1998).
53. R. M. Laine and A. Sellinger, United States Patent 6,551,960 B1 (2003).
54. Y. Wang, J. Ren, K. Deng, L. Gui, and Y. Tang, *Chem. Mater.* 12, 1622 (2000).
55. X. Zhang and K.-Y. Chan, *Chem. Mater.* 15, 451 (2003).
56. Z. L. Liu, X. Y. Ling, J. Y. Lee, X. D. Su, and L. M. Gan, *J. Mat. Chem.* 13, 3049 (2003).
57. Z. H. Zhou, S. L. Wang, W. J. Zhou, G. X. Wang, L. H. Jiang, W. Z. Li, S. Q. Song, J. G. Liu, G. Q. Sun, and Q. Xin, *Chem. Commun.* 3, 394 (2003).
58. C. Bock, C. Paquet, M. Couillard, G. Button, and B. MacDougall, *J. Am. Chem. Soc.* 126, 8028 (2004).
59. J. W. Gou, T. S. Zhao, J. Prabhuram, and C. W. Wong, *Electrochim. Acta* 50, 1973 (2005).
60. S. Floate, M. Hosseini, M. R. Arshadi, D. Ritson, K. L. Young, and R. J. Nichols, *J. Electroanal. Chem.* 542, 67 (2003).
61. S. F. Huang, Y. Chi, C. Bock, B. MacDougall, and A. Carty, *J. Chem. Vapor Dep.* 3, 9 (2003).
62. C. K. Witham, W. Chun, T. I. Valdez, and S. R. Narayanan, *Electrochem. Solid State Lett.* 3, 497 (2000).
63. M. C. Denis, G. Lalande, D. Guay, J. P. Dodelet, and R. Schulz, *J. Appl. Electrochem.* 29, 951 (1999).
64. M. S. Nashner, A. I. Frenkel, D. L. Adler, J. R. Shapley, and R. G. Nuzzo, *J. Am. Chem. Soc.* 33, 119 (1997).
65. M. S. Nashner, A. I. Frenkel, D. Sommerville, C. W. Hills, J. R. Shapley, and R. G. Nuzzo, *J. Am. Chem. Soc.* 120, 8093 (1998).
66. C. Pan, F. Dassenoy, M. J. Casanove, K. Philippot, C. Amiens, P. Lecante, A. Mosset, and B. Chaudret, *J. Phys. Chem. B* 103, 10 098 (1999).
67. K. Moseley and P. M. Maitlis, *J. Chem. Soc. Commun.* 52, 982 (1971).
68. P. Portuci and G. Vituli, *Inorg, Synth.* 22, 178 (1983).
69. M. Harada, N. Toshima, K. Yoshida, and S. Isoda, *J. Colloid Interface Sci.* 283, 64 (2005).
70. F. Dassenoy, M. J. Casanove, P. Lecante, C. Pan, K. Philippot, C. Amiens, and B. Chaudret, *J. Phys. Rev. B* 63, 5407 (2001).
71. S. R. Brankovic, J. X. Wang, and R. R. Adzic, *Surf. Sci.* 474, L173 (2001).
72. S. R. Brankovic, J. McBreen, and R. R. Adzic, *J. Electroanal. Chem.* 503, 99 (2001).
73. S. R. Brankovic, J. X. Wang, and R. R. Adzic, *Electrochem. Solid State Lett.* 4, A217 (2001).
74. H. Inoue, S. R. Brankovic, J. X. Wang, and R. R. Adzic, *Electrochim. Acta* 47, 3777 (2002).
75. J. X. Wang, S. R. Brankovic, Y. Zhu, J. C. Hanson, and R. R. Adzic, *J. Electrochem. Soc.* 150, A1108 (2003).
76. K. Sasaki, J. X. Wang, M. Balasubramanaian, J. McBreen, F. Uribe, and R. R. Adzic, *Electrochim. Acta* 49, 3873 (2004).
77. J. Zhang, Y. Mo, M. B. Vukmirovic, R. Klie, K. Sasaki, and R. R. Adzic, *J. Phys. Chem. B* 108, 10 955 (2004).
78. S. T. Kuk and A. Wieckoski, *J. Power Source* 141, 1 (2005).
79. K. A. Friedrich, K.-P. Geyzers, A. Marmann, U. Stimming, and R. Vogel, *Z. Phys. Chem.* 208, 137 (1999).
80. H. Kim, I. R. de-Morales, G. Tremiliosi, R. Haasch, and A. Wieckoswki, *Surf. Sci.* 474, L203 (2001).
81. A. Crown, I. R. Moraes, and A. Wieckoswki, *J. Electroanal. Chem.* 500, 333 (2001).
82. F. Maillard, G.-Q. Lu, A. Wieckowski, and U. Stimming, *J. Phys. Chem. B* 109, 16 230 (2005).
83. S. Strbac, C. M. Johnston, G. Q. Lu, A. Crown, and A. Wieckoswki, *Surf. Sci.* 573, 80 (2004).
84. P. K. Babu, H. S. Kim, J. H. Chung, E. Oldfield, and A. Wieckoswki, *J. Phys. Chem. B* 108, 20 228 (2004).
85. H. Hoster, T. Iwasita, H. Baumgartner, and W. Vielstich, *Phys. Chem. Chem. Phys.* 3, 337 (2001).
86. J. Luo, M. M. Mave, Y. B. Lou, L. Han, M. Hepel, and C. J. Zhong, *Catal. Today* 77, 127 (2002).
87. M. S. El-Deab and T. Ohsaka, *J. Electroanal. Chem.* 553, 107 (2003).
88. J. Luo, M. M. Mave, N. N. Kariuki, L. Y. Wang, P. Nioki, Y. Lin, M. Schadt, H. R. Naslund, and C. J. Zhong, *Catal. Today* 99, 291 (2005).
89. K. Matsuoka, Y. Irivama, A. A. Takeshi, M. B. Masao, and Z. Ogumi, *J. Electrochem. Soc.* 152, A729 (2005).
90. G. Gokagac and B. J. Kennedy, *Z. Naturforsch. Sect. B. J. Chem. Sci.* 57, 193 (2002).
91. L. X. Yang, C. Bock, B. MacDougall, and J. Park, *J. Appl. Electrochem.* 34, 427 (2004).
92. P. K. Shen and A. C. C. Tseung, *J. Electrochem. Soc.* 141, 3082 (1994).
93. A. K. Shukla, M. K. Ravikumar, A. S. Arico, G. Candiano, V. Antonucci, N. Giordano, and A. Hamnett, *J. Appl. Electrochem.* 25, 528 (1995).
94. M. Gotz and H. Wendt, *Electrochim. Acta* 43, 3637 (1998).
95. H. Q. Zhang, Y. Wang, E. R. Fachini, and C. R. Cabrera, *Electrochem. Solid State Lett.* 2, 437 (1999).
96. A. L. N. Pinheiro, A. Oliveira-Neto, E. C. de-Souza, J. Perez, V. A. Paganin, E. A. Ticianelli, and E. R. Gonzalez, *J. New Mater. Electrochem. Sys.* 6, 1 (2003).
97. K. Wang, H. A. Gasteiger, N. M. Markovic, and P. N. Ross, *Electrochim. Acta* 41, 2587 (1996).
98. S. Mukerjee and J. McBreen, *J. Electrochem. Soc.* 146, 600 (1999).
99. G. Gokagac, J. M. Leger, and F. Hahn, *Z. Naturforsch. Sect. B. J. Chem. Sci.* 58, 423 (2003).
100. A. C. Chen, D. J. La Russa, and B. Miller, *Langmuir* 20, 9695 (2004).
101. K. W. Park, J. H. Choi, S. A. Lee, C. Pak, H. Chang, and Y. E. Sung, *J. Catal.* 224, 236 (2004).
102. F. Liu, J. Y. Lee, and W. J. Zhou, *J. Phys. Chem. B* 108, 17 959 (2004).
103. S. Mukerjee and R. C. Urian, *Electrochim. Acta* 47, 3219 (2002).
104. S. Mukerjee, R. C. Urian, S. J. Lee, E. A. Ticianelli, and J. McBreen, *J. Electrochem. Soc.* 151, A1094 (2004).
105. H. Boennemann, R. Brinkmann, P. Britz, U. Endruschat, R. Mortel, U. A. Paulus, G. J. Feldmeier, T. J. Schmidt, H. A. Gasteiger, and R. J. Behm, *J. New Mater. Electrochem. Systems* 3, 199 (2000).

106. V. Radmilovic, T. J. Richardson, S. J. Chen, and P. N. Ross, *J. Catal.* 232, 199 (2005).
107. E. M. Crabb, R. Marshall, and D. Thompsett, *J. Electrochem. Soc.* 147, 4440 (2000).
108. H. Gasteiger, N. Markovic, and P. Ross, *Catal. Lett.* 36, 1 (1996).
109. T. J. Schmidt, Z. Jusys, H. A. Gasteiger, R. J. Behm, U. Endruschat, and H. Boennemann, *J. Electroanal. Chem.* 501, 132 (2001).
110. C. Bock and B. MacDougall, *J. Electrochem. Soc.* 150, E377 (2003).
111. C. Bock, M. A. Blakely, and B. MacDougall, *Electrochim. Acta* 50, 2401 (2005).
112. C. Bock, A. Collier, and B. MacDougall, *J. Electrochem. Soc.*, in press.
113. S. Adora, J.-P. Simon, Y. Soldo-Olivier, R. Faure, E. Chainet, and R. Durand, *ChemPhysChem* 5, 1178 (2004).
114. J. Munk, P. A. Christensen, A. Hamnett, and E. Skou, *J. Electroanal. Chem.* 401, 215 (1996).
115. K. A. Friedrich, F. Henglein, U. Stimming, and W. Unkauf, *Electrochim. Acta* 45, 3283 (2000).
116. S. Park and M. J. Weaver, *J. Phys. Chem. B* 106, 8667 (2002).
117. S.-M. Moon, C. Bock, and B. MacDougall, *J. Electroanal. Chem.* 568, 225 (2004).
118. V. Stamenkovic, M. Arenz, P. N. Ross, and N. M. Markovic, *J. Phys. Chem.* 108, 17 915 (2004).
119. C. Rice, Y. Tong, E. Oldfield, A. Wieckowski, F. Hahn, F. Gloaguen, J. M. Leger, and C. Lamy, *J. Phys. Chem. B* 104, 5803 (2000).
120. S. Park, Y. Xie, and M. J. Weaver, *Langmuir* 18, 5792 (2002).
121. M. Arenz, K. J. J. Mayrhofer, V. Stamenkovic, B. B. Blizanac, T. Tomoyuki, P. N. Ross, and N. M. Markovic, *J. Am. Chem. Soc.* 127, 6819 (2005).
122. L. N. Lewis and N. Lewis, *J. Am. Chem. Soc.* 108, 7228 (1986).
123. M. R. Mucalo and R. P. Cooney, *J. Chem. Soc., Chem. Commun.* 2, 94 (1989).
124. J. S. Bradley, J. M. Millan, E. W. Hill, S. Behal, B. Chaudret, and A. Duteil, *Faraday Discuss. Chem. Soc.* 92, 255 (1991).
125. M. R. Mucalo and R. P. Cooney, *Chem. Mater.* 3, 1081 (1991).
126. A. Duteil, R. Queau, B. Chaudret, R. Mazel, C. Rouceau, and J. S. Bradley, *Chem. Mater.* 5, 341 (1993).
127. D. deCaro and J. S. Bradley, *Langmuir* 13, 3067 (1997).
128. D. deCaro, and J. S. Bradley, *Langmuir* 14, 245 (1998).
129. D. deCaro and J. S. Bradley, *New J. Chem.* 22, 1267 (1998).
130. S. Park, S. A. Wasileski, and M. J. Weaver, *J. Phys. Chem. B* 105, 9719 (2001).
131. R. G. Greenler, K. D. Burch, K. Kretzschmar, R. Klauser, A. M. Bradshew, and B. E. Hayden, *Surf. Sci.* 338, 152 (1985).
132. P. Hollins, *Surf. Sci. Rep.* 16, 51 (1992).
133. M. J. Kappers and J. H. van der Maas, *Catal. Lett.* 10, 365 (1991).
134. B. Hammer, O. H. Nielson, and J. K. Norskov, *Catal. Lett.* 46, 31 (1997).
135. J. Fraissard, *Catal. Today* 51, 481 (1999).
136. Y. Y. Tong, C. Rice, A. Wieckowski, and E. Oldfield, *J. Am. Chem. Soc.* 122, 1123 (2000).
137. P. K. Balm, H. S. Kim, E. Oldfield, and A. Wieckowski, *J. Phys. Chem. B* 107, 7595 (2003).
138. D. Wabner and C. Grambow, *J. Electroanal. Chem.* 195, 95 (1985).
139. J. Feng and D. C. Johnson, *J. Electrochem. Soc.* 138, 3328 (1991).
140. R. Kotz, S. Stucki, and B. Carcer, *J. Appl. Elecchem.* 21, 14 (1991).
141. S. Stucki, R. Kotz, B. Carcer, and W. Suter, *J. Appl. Elecchem.* 21, 99 (1991).
142. M. Gatrell and D. Kirk, *J. Electrochem. Soc.* 139, 2736 (1992).
143. C. Comninellis and C. Pulgarin, *J. Appl. Elecchem.* 21, 703 (1991).
144. C. Pulgarin, N. Adler, P. Peringer, and C. Comninellis, *Water Res.* 4, 887 (1994).
145. C. Comninellis, *Electrochim. Acta* 39, 1857 (1994).
146. C. Comninellis and A. De Battisti, *J. Chim. Phys.* 83, 673 (1996).
147. O. Simond, V. Schaller, and C. Comninellis, *Electrochim. Acta* 42, 2009 (1997).
148. B. Correa-Lozano, C. Comninellis, and A. DeBattisti, *J. Appl. Electrochem.* 27, 970 (1997).
149. C. Bock and B. MacDougall, *Electrochim. Acta* 47, 3361 (2002).
150. C. Bock, A. Smith, and B. MacDougall, *Electrochim. Acta* 48, 57 (2002).
151. P. K. Shen and A. C. C. Tseung, *J. Mater. Chem.* 2, 1141 (1992).
152. M. P. Soriaga, E. Binamira-Soriaga, A. T. Hubbard, J. B. Benziger, and K. W. P. Pang, *Inorg. Chem.* 24, 65 (1985).
153. C. Bock and B. MacDougall, *J. Electroanal. Chem.* 491, 48 (2000).
154. I. Duo, S. Ferro, A. DeBattisti, and C. Comninellis, in "Catalysis and Electrocatalysis at Nanoparticle Surfaces" (A. Wieckowski, E. R. Savinova, and C. G. Vayenas, Eds.), p. 877. Marcel Dekker, Inc., New York, Basel, 2003.
155. C. G. Vayenas, S. Bebelis, C. Pliangos, S. Brosda, and D. Tsiplakides, "Electrochemical Activation of Catalysis: Promotion, Electrochemical Promotion and Metal-Support Interactions." Kluwer Academic/Plenum Publishers, New York, 2001.
156. R. M. Lambert, F. Williams, A. Palermo, and M. S. Tikhov, *Top. Catal.* 13, 91 (2000).
157. R. Wuthrich, E. A. Baranova, H. Bleuler, and C. Comninellis, *Electrochem. Commun.* 6, 1199 (2004).
158. E. A. Baranova, G. Foti, and C. Comninellis, *Electrochem. Commun.* 6, 389 (2004).
159. E. A. Baranova, A. Thursfield, S. Brosda, G. Foti, C. Comninellis, and C. G. Vayenas, *J. Electrochem. Soc.* 152, E40 (2005).
160. J. O. Bockris and J. Kim, *J. Appl. Electrochem.* 27, 623 (1997).
161. A. C. A. de Voovs, R. A. Santen, and J. A. R. van Veen, *J. Mol. Catal. A Chem.* 154, 203 (2000).
162. D. De, J. D. Englehardt, and E. E. Kalu, *J. Electrochem. Soc.* 147, 4224 (2000).
163. F. Gauthard, F. Epron, and J. Barbier, *J. Catal.* 220, 182 (2003).
164. D. De, E. E. Kalu, P. P. Tarjan, and J. D. Englehardt, *Chem. Eng. Technol.* 27, 56 (2004).
165. P. M. Tucker, M. J. Waite, and B. E. Hayden, *J. Appl. Electrochem.* 34, 781 (2004).
166. R. L. Augustin, "Catalytic Hydrogenation." Dekker, New York, 1965.
167. J. M. Chapuzet, A. Lasia, and J. Lessard, in "Electrocatalysis" (J. Lipkowski and P. N. Ross, Eds.), p. 155. Wiley-VCH, New York, 1998.
168. L. D. Burke, C. Kemball, and F. A. Lewis, *Trans. Faraday Soc.* 60, 913 (1964).
169. M. Byrne and A. T. Kuhn, *J. Chem. Soc. Faraday I* 68, 355 (1972).
170. S. H. Langer and G. P. Sakellaropoulos, *J. Electrochem. Soc.* 122, 1619 (1975).
171. J.-C. Moutet, *Org. Prep. Proced. Int.* 24, 309 (1992).
172. L. L. Miller and L. Christensen, *J. Org. Chem.* 43, 2059 (1978).
173. K. Amouzegar and O. Savadogo, *Electrochim. Acta* 39, 557 (1994).
174. P. B. Janardhanan, *J. Sci. Ind. Res.* 12B, 183 (1953).
175. B. Sakurai and T. Arai, *Bull. Chem. Soc. Jpn.* 28, 93 (1955).
176. G. Belot, S. Desjardins, and J. Lessard, *Tetrahedron Lett.* 25, 5347 (1984).
177. J. Lessard and G. Belot, United States Patent 4,584,069 (1986).
178. M. A. Casedei and D. Pletcher, *Electrochim. Acta* 33, 117 (1988).
179. A. Cyr, P. Huot, G. Belot, and J. Lessard, *Electrochim. Acta* 35, 147 (1990).